

Bridging Econometrics and AI: VaR Estimation via Reinforcement Learning and GARCH Models

Fredy POKOU ^{*1}, Jules SADEFO KAMDEM ^{†2}, and François BENHMAD ^{‡3}

¹Inria, CNRS, Univ. of Lille, Centrale Lille, UMR 9189 - CRISTAL, F-59000 Lille, France
^{2,3}MRE UR 209 and Faculty of Economics. Montpellier University, France

August 19, 2025

Abstract

Estimating market risk in volatile environments remains a major challenge, as traditional GARCH-type models often struggle to capture nonlinear dynamics. This paper proposes a hybrid Value-at-Risk (VaR) framework that integrates GARCH volatility forecasts with a Double Deep Q-Network (DDQN) reinforcement learning classifier. By reframing VaR estimation as a classification problem, the model adaptively adjusts risk thresholds based on predicted low- and high-risk return regimes. Using more than 16 years of Euro Stoxx 50 data, the framework achieves 79.4% test accuracy and substantially reduces both the frequency and the temporal clustering of VaR violations. Backtesting confirms compliance with the Kupiec and Christoffersen tests, while Extreme Value Theory supports its ability to model tail risk. The resulting approach offers a statistically robust, capital-efficient, and regulatory-aligned solution for proactive financial risk management.

Keywords: Deep reinforcement learning, Directional prediction, Imbalanced class problem, Value-at-Risk.

1 Introduction

Context: Forecasting stock returns is a long-standing challenge in financial economics, with significant implications for both risk management and regulatory compliance. Traditional econometric models such as GARCH (Bollerslev, 1986) capture volatility persistence but fail to fully account for key stylized facts of financial time series: fat tails, volatility clustering, and leverage effects (Glosten et al., 1993). Similarly, modern machine learning and deep learning methods, although capable of modeling nonlinear dynamics (Goodfellow et al., 2016; Tealab, 2018), tend to underperform during rare but impactful market shocks (Fawcett and Provost, 1997; Pokou, 2022). As illustrated in Figure 1, these limitations often result in systematic mispredictions of excess returns, especially in turbulent markets. These forecasting inaccuracies are critical because they directly translate into unreliable estimates of Value-at-Risk (VaR), the benchmark risk measure under Basel regulatory frameworks (on Banking Supervision, 2017). Overestimation inflates capital requirements, whereas underestimation exposes institutions to excessive losses. To mitigate these shortcomings, the recent literature has shifted from precise return forecasting to directional return prediction, reframe the task as a classification problem, determining whether returns will be positive or negative (Kanas, 2001; Nyberg, 2011; Alstad and Davulcu, 2017). Beyond the standard zero threshold, quantile and volatility-based criteria have been introduced to better isolate significant market movements (Chung and Hong, 2007; Linton and Whang, 2007).

^{*}fredypokou@gmx.fr

[†]jules.sadefo-kamdem@umontpellier.fr

[‡]francois.benhmad@umontpellier.fr

Building on this line of research, we follow [Nevasalmi \(2020\)](#) in adopting a finer classification that filters noise and emphasizes extreme outcomes. Although this approach improves the alignment between forecasts and risk exposure, it introduces a severe class imbalance problem, a largely unexplored challenge in the financial risk literature.

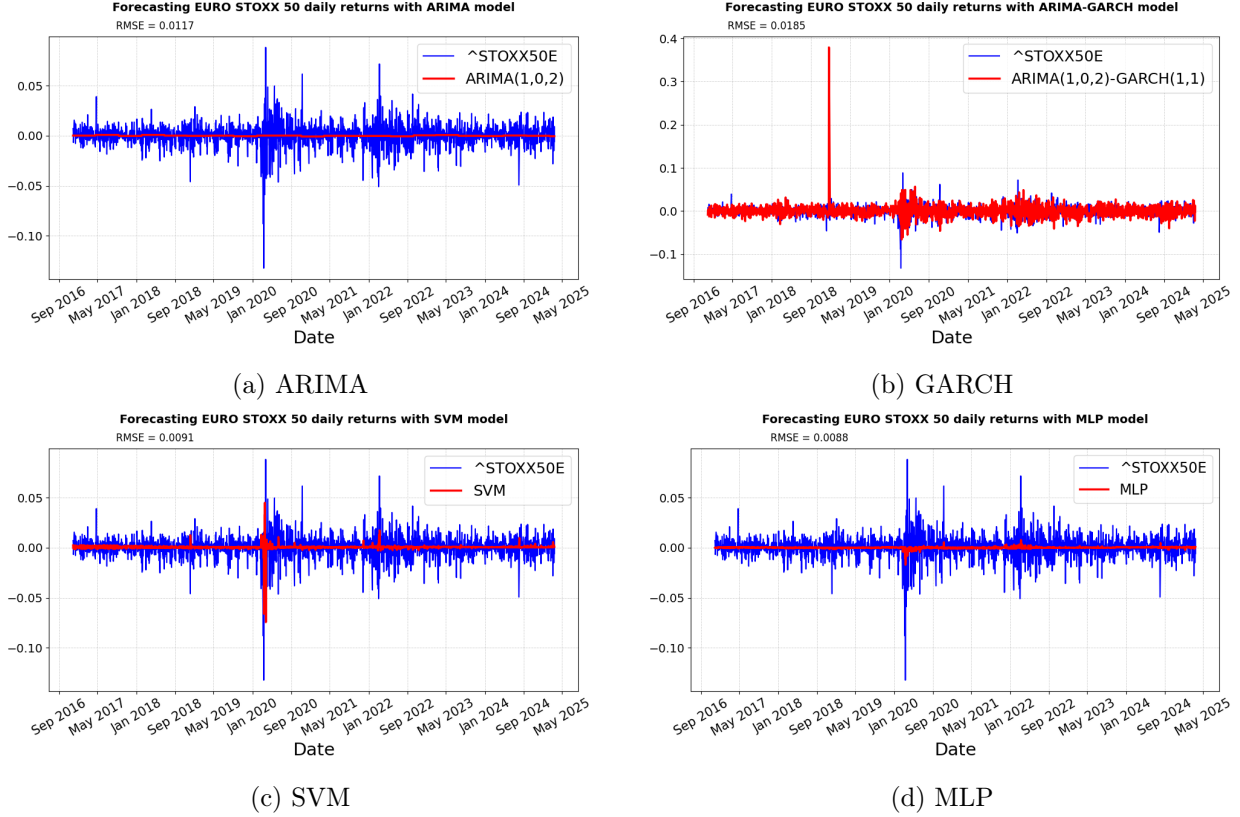


Figure 1: Euro Stoxx 50 return forecasts using different models

Problem Statement: The central challenge of this study is the reliable estimation of the Value-at-Risk (VaR) when the return prediction is reformulated as a directional prediction task under volatile market conditions. In practice, extreme negative returns are the outcomes most critical for risk management and regulatory compliance, but they occur far less frequently than small or positive returns. This structural asymmetry, known as the imbalanced class problem, undermines the predictive capacity of both econometric models and supervised machine learning techniques, often leading to systematic underestimation of VaR and, consequently, potential regulatory breaches. To address this imbalance, researchers have developed various data rebalancing strategies. Among oversampling methods, the widely used Synthetic Minority Oversampling Technique (SMOTE) ([Chawla et al., 2002](#)) creates synthetic minority observations to enhance classifier sensitivity, while Borderline-SMOTE ([Han et al., 2005](#)) focuses on generating synthetic data near decision boundaries. On the undersampling side, Tomek Links ([Tomek, 1976](#); [Elhassan and Aljurf, 2016](#)) remove borderline majority instances, whereas Edited Nearest Neighbors (ENN) ([Wilson, 2007](#); [Elhassan and Aljurf, 2016](#)) eliminate misclassified majority samples to improve class separability. More recent hybrid techniques combine oversampling and undersampling, for example, SMOTE with Tomek Links to improve balance while reducing noise ([Zeng et al., 2016](#); [Pereira et al., 2020](#); [Tang et al., 2008](#)). Furthermore, cost-sensitive learning penalizes errors in minority outcomes more heavily, encouraging models to better capture rare but impactful returns ([Tang et al., 2008](#)). Despite their contributions, these methods often introduce bias or overfitting, particularly in financial contexts where return distributions evolve rapidly and exhibit strong nonlinear dynamics. As a result, conventional rebalancing remains insufficient for adaptive risk forecasting. Against this backdrop, Deep Reinforcement Learning (DRL) offers a promising alternative. Unlike static rebalancing techniques, DRL learns an adaptive policy that continuously adjusts to market conditions while explicitly addressing class imbalance ([Mnih et al., 2013](#); [Van Hasselt et al., 2016](#); [Yang et al., 2020](#)).

By reformulating stock return forecasting, which was previously a regression problem, into a directional forecasting framework in a context of class imbalance, our approach aims to provide more robust and regulatory-relevant VaR estimates.

Main Contributions: This paper advances the literature on financial risk modeling by proposing a novel hybrid framework for Value-at-Risk (VaR) estimation that explicitly addresses the challenges of volatility dynamics and class imbalance in directional prediction.

First, based on the recent work of [Nevasalmi \(2020\)](#), we reformulate return prediction as a directional prediction problem, adopting refined thresholds that better isolate extreme returns and filter out noise. This formulation improves the model's sensitivity to rare but economically significant market movements, a dimension often neglected by conventional approaches. Second, we develop a hybrid econometric AI methodology that combines the volatility modeling strengths of the GARCH family with the adaptive capabilities of Deep Reinforcement Learning (DRL). Unlike static machine learning classifiers, DRL enables dynamic policy adjustment, thus directly addressing the imbalanced class problem and improving robustness in turbulent market environments. Third, we highlight the regulatory and economic relevance of our approach. By reducing both the frequency of VaR violations and the associated capital requirements, the framework provides a risk management tool that is better aligned with the prudential standards of Basel III, mitigating the twin risks of overcapitalization and underestimation of losses. Finally, we present a rigorous empirical validation using daily Eurostoxx 50 data that cover periods of increased volatility and financial crisis. The results demonstrate that our approach outperforms traditional econometric and supervised learning models in terms of accuracy, stability, and robustness, offering a more reliable foundation for proactive risk management.

Reviewed Literature: Value-at-risk (VaR) estimation has long relied on econometric approaches such as the GARCH family ([Bollerslev, 1986](#); [Glosten et al., 1993](#)), which, despite their analytical rigor, often fail to capture heavy tails, volatility clustering, and leverage effects. To address these limitations, machine learning methods, including neural networks and ensemble models, have been applied to financial time series ([Zhang, 2003](#); [Tealab, 2018](#); [Pokou et al., 2024](#)). Although such models improve non-linear predictive capacity, they remain sensitive to class imbalance and tend to underestimate rare but impactful shocks.

In recent years, risk-sensitive reinforcement learning (RL) has attracted considerable attention as a means of embedding robustness into decision making under uncertainty. [Morimura et al. \(2012\)](#) introduced parametric return density estimation through a risk-sensitive Bellman framework, while [Ying et al. \(2022\)](#) proposed a CVaR-constrained policy optimization algorithm that ensures safety by explicitly controlling downside risk. Extending this line, [Noorani et al. \(2025\)](#) formulated a risk-sensitive actor-critical method using exponential criteria to improve robustness and sample efficiency. Similarly, [Zhang et al. \(2024\)](#) developed CVaR-Constrained Policy Optimization (CVaR-CPO) to ensure safety in reinforcement learning by focusing on the upper tail of cost distributions. In the context of asset allocation, [Cui et al. \(2023\)](#) employed a CVaR-based deep reinforcement learning approach for cryptocurrency portfolios, demonstrating the superiority of DRL in environments with large tail risks.

From a distributional perspective, [Stanko and Macek \(2019\)](#) advanced CVaR Q-learning, reducing computational complexity and highlighting the relevance of distributional RL for risk-averse policy design. Although these contributions significantly advance risk-sensitive RL and CVaR-based methodologies, they primarily focus on direct quantile estimation, risk-sensitive optimization, or portfolio allocation problems. In contrast, our study introduces a fundamentally different perspective by reformulating the VaR estimation as a directional forecasting problem. Inspired by [Nevasalmi \(2020\)](#), we adopt refined thresholds to isolate extreme returns and explicitly address the resulting class imbalance through Deep Reinforcement Learning. Combined with GARCH volatility modeling, our hybrid framework offers a more adaptive and regulatory-relevant approach, combining econometric rigor with the flexibility of DRL in a way that has not yet been explored in the literature.

Paper Organization: The remainder of the paper is structured as follows. Section 2 introduces the methodological framework, including the GARCH modeling and the DRL architecture for adaptive VaR estimation. Sections 3 and 4 present the empirical validation of Eurostoxx 50 daily data, discussing robustness checks and comparative analysis. Section 5 concludes with the main findings, policy implications, and avenues for future research.

2 Methodology

Let P_t be the closing price of an asset at time t , so the logarithmic return at time t over a unit time interval is defined as $r_t = \log(P_t/P_{t-1})$.

2.1 Value-at-Risk

The Value-at-Risk (VaR) at confidence level α is defined as the α -quantile of the return distribution and represents the loss that will be exceeded in $\alpha \times 100\%$ of cases over the next period. Formally,

$$P(r_{t+1} < -VaR_{t+1}^\alpha) = \alpha, \quad (1)$$

where $\alpha \in [0, 1]$ is typically set to 0.05 or 0.01 in risk management applications. Denoting by $F_{r_{t+1}}(\cdot)$ the cumulative distribution function (CDF) of returns, the VaR can equivalently be expressed as

$$VaR_{t+1}(\alpha) = -F_{r_{t+1}}^{-1}(\alpha), \quad (2)$$

where $F_{r_{t+1}}^{-1}(\alpha)$ is the inverse CDF of a continuous probability distribution, or quantile function, of r_{t+1} .

Although nonparametric estimation of $F_{r_{t+1}}^{-1}$ is possible, parametric VaR remains widely used in practice due to its simplicity and its ability to incorporate stylized facts of financial returns, such as heavy tails, volatility clustering, and asymmetry (Glosten et al., 1993). A common starting point is the conditional location scale representation.

$$r_{t+1} = \mu_{t+1} + \sigma_{t+1} z_{t+1}, \quad (3)$$

where μ_{t+1} and σ_{t+1} are the conditional mean and volatility, and z_{t+1} is an i.i.d. innovation with zero mean and unit variance. Under this specification, the one-step-ahead VaR at level α takes the unified form

$$VaR_{t+1}(\alpha) = -\mu_{t+1} + \sigma_{t+1} F_{z_{t+1}}^{-1}(\alpha), \quad (4)$$

where $F_{z_{t+1}}^{-1}(\alpha)$ denotes the α -quantile of the standardized innovation distribution. For innovations in standard normal distribution, $F_{r_{t+1}}^{-1}(\alpha) = \Phi^{-1}(\alpha)$, while for heavy-tailed data, a standard Student t distribution with ν degrees of freedom is often preferred, resulting in $F_{z_{t+1}}^{-1}(\alpha) = t_\nu^{-1}(\alpha)$.

In practice, the conditional mean μ_{t+1} of daily returns is close to zero and is commonly modeled as a constant. However, conditional volatility σ_{t+1} is dynamic and is typically estimated using generalized autoregressive conditional heteroskedasticity models, such as GARCH(p,q) (Bollerslev, 1986) or its asymmetric extensions, including GJR-GARCH (Glosten et al., 1993). These models capture the persistence and clustering of volatility, while the choice of distribution for z_t accounts for the fat tails frequently observed in financial data.

2.2 GARCH models

Introduced by Bollerslev (1986), the GARCH(p,q) model can be defined by assuming that $\{r_t\}_{t \in \mathbb{N}}$ is a stochastic process decomposable in terms of expected returns and residuals, as follows:

$$r_t = \mu_t + \epsilon_t$$

where

$$\begin{cases} \epsilon_t = \sigma_t z_t, \\ \sigma_t^2 = \alpha_0 + \sum_{i=1}^p \alpha_i \epsilon_{t-i}^2 + \sum_{j=1}^q \beta_j \sigma_{t-j}^2, \end{cases} \quad (5)$$

where z_t is an innovation standardized by i.i.d. with zero mean and unit variance. The positivity of the conditional variance is ensured by $\alpha_0 > 0$, $\alpha_i \geq 0$, and $\beta_j \geq 0$, while weak stationarity requires $\sum_{i=1}^p \alpha_i + \sum_{j=1}^q \beta_j < 1$.

The GARCH (1,1) model is the simplest and most commonly used univariate model and can be defined as follows:

$$\begin{cases} \epsilon_t = \sigma_t z_t \\ \sigma_t^2 = \alpha_0 + \alpha_1 \epsilon_{t-1}^2 + \beta_1 \sigma_{t-1}^2 \end{cases} \quad (6)$$

where the variance process σ_t^2 in GARCH(1,1) is stationary when $\alpha_1 + \beta_1 < 1$.

The convergence rate depends on $\alpha_1 + \beta_1$. As persistence is closer to 1, it takes longer for a shock to be forgotten by the market.

[Glosten, Jagannathan, and Runkle \(1993\)](#) proposed the GJR-GARCH(p,q) model to overcome GARCH's inability to differentiate between negative and positive shocks and to take leverage into account. It can be defined as follows:

$$\begin{cases} \epsilon_t = \sigma_t z_t \\ \sigma_t^2 = \alpha_0 + \sum_{i=1}^p (\alpha_i + \gamma_i \mathbb{1}_{\epsilon_{t-i} < 0}) \times \epsilon_{t-i}^2 + \sum_{j=1}^q \beta_j \sigma_{t-j}^2 \end{cases} \quad (7)$$

In particular, GJR-GARCH(1,1) is expressed as follows:

$$\begin{cases} \epsilon_t = \sigma_t z_t \\ \sigma_t^2 = \alpha_0 + (\alpha_1 + \gamma \mathbb{1}_{\epsilon_{t-1} < 0}) \times \epsilon_{t-1}^2 + \beta_1 \sigma_{t-1}^2 \end{cases} \quad (8)$$

where z_t is an innovation standardized by i.i.d. and $\mathbb{1}_{\{\epsilon_{t-1} < 0\}}$ is an indicator function that equals one if the lagged innovation is negative ("bad news") and zero otherwise. This formulation allows negative shocks to exert a disproportionately larger effect on conditional variance when $\gamma > 0$, thus modeling the well-documented leverage effect. The possibility of conditional variance is guaranteed when $\alpha_0 > 0$, $\alpha_1 \geq 0$, $\beta_1 \geq 0$, and $\alpha_1 + \gamma \geq 0$. The stationarity of the variance process is further ensured under the condition $\alpha_1 + \beta_1 + \frac{1}{2}\gamma < 1$. This specification thus provides a parsimonious yet effective framework for accommodating asymmetries in volatility dynamics, a key feature of financial return series.

Although there are numerous extensions of the GARCH framework, such as EGARCH, TGARCH, and APARCH, our analysis focuses on the standard GARCH and its asymmetric variant, GJR-GARCH. These models capture the essential stylized facts of financial returns, namely volatility clustering, persistence, heavy tails, and leverage effects. Furthermore, restricting attention to GARCH and GJR-GARCH ensures parsimony and avoids the risk of overparameterization, which is particularly relevant in high-frequency estimation and reinforcement learning contexts. This balance between explanatory power and tractability makes them a robust baseline for integrating econometric volatility modeling with adaptive reinforcement learning techniques.

2.3 Threshold selection for directional prediction

In the context of directional forecasting, the choice of threshold c is critical for transforming continuous returns into binary outcomes. Although simple strategies often adopt $c = 0$ to distinguish between positive and negative returns ([Kanas, 2001](#); [Nyberg, 2011](#)), our objective to improve Value-at-Risk (VaR) estimation requires a more risk-sensitive criterion. Specifically, we define c as the most severe threshold associated with observed VaR violations over a given horizon H . Formally, let k index the time periods within the horizon.

Then,

$$c = \max \{ r_{k+1} \mid r_{k+1} < \text{VaR}_{k+1}(\alpha), k = 1, \dots, H \}. \quad (9)$$

Since $\text{VaR}_{k+1}(\alpha)$ is typically negative, this definition ensures that c corresponds to the least negative return among the set of violations, i.e. the 'mildest' loss still affecting the VaR limit. The binary outcome variable is then constructed as

$$y_t(c) = \mathbb{1}_{\{r_t \leq c\}}, \quad (10)$$

which flags return less than or equal to c as high-risk outcomes.

This formulation explicitly links the classification threshold to the realized downside risk, aligning the directional prediction with the practical objective of reducing VaR violations.

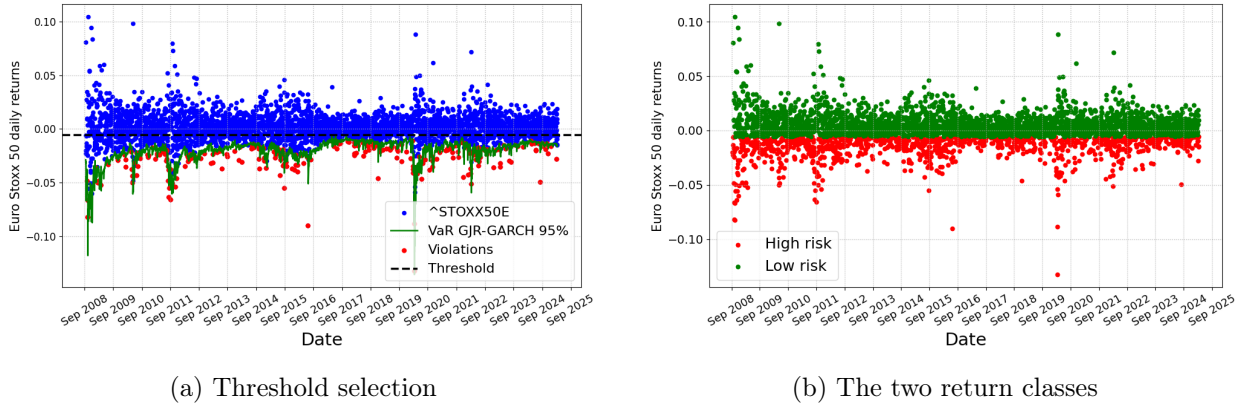


Figure 2: Illustration characterization of threshold and return classes

Figure 2 illustrates our threshold-based approach for the directional prediction of returns. The panel 2a depicts the dynamic selection of the risk threshold c , defined as the least severe loss among recent VaR violations, ensuring that the classification criterion is directly anchored in the realized downside risk. This adaptive procedure allows the threshold to evolve with market conditions, reflecting the gravity of observed losses. The panel 2b translates this threshold into a binary classification of returns: outcomes at or below c are labeled high-risk ($y_t(c) = 1$), while all others are labeled low-risk ($y_t(c) = 0$). These panels demonstrate how linking threshold selection to actual VaR breaches provides a more sensitive and operationally relevant framework to distinguish between high- and low-risk periods, thus enhancing the predictive capacity of risk management models.

2.4 Proposed VaR model

Let $\text{VaR}_{t+1}(\alpha)$ denotes the advance value at risk in one step at the confidence level α , estimated by a GARCH or GJR-GARCH process. We introduce a classification model that, at each time $t + 1$, assigns the portfolio to one of two states:

- Low risk: corresponding to a lower level of downside exposure;
- High risk: corresponding to a heightened level of downside exposure.

We then define an adjusted risk measure as follows.

Definition 1 (Classification-Adjusted Value at Risk). *The Classification-Adjusted Value-at-Risk denoted $\text{VaR}_{ML}(\alpha)$, is given by*

$$\text{VaR}_{ML}(\alpha) = \begin{cases} (1 - b_1) \cdot \text{VaR}_{t+1}(\alpha), & \text{if } \hat{r}_{t+1} = \text{"Low risk"}, \\ (1 + b_2) \cdot \text{VaR}_{t+1}(\alpha), & \text{if } \hat{r}_{t+1} = \text{"High risk"}, \end{cases} \quad (11)$$

where $b_1, b_2 \in \mathbb{R}^+$ are calibration parameters controlling the degree of adjustment, and \hat{r}_{t+1} denotes the predicted risk category.

Proposition 2.1. *The Classification-Adjusted Value-at-Risk, $\text{VaR}_{ML}(\alpha)$, preserves the fundamental properties of the original Value-at-Risk.*

Proof. Recall that the Value-at-Risk is positively homogeneous, that is, for any $\lambda \geq 0$,

$$\text{VaR}_{t+1}^{\lambda X}(\alpha) = \lambda \cdot \text{VaR}_{t+1}^X(\alpha).$$

In our framework, the adjustment factor applied to $\text{VaR}_{t+1}(\alpha)$ is either $(1 - b_1)$ or $(1 + b_2)$, depending on the classification outcome. Since \hat{r}_{t+1} takes a single value in Low risk, High risk, only one branch of the definition is active at any given time, ensuring that

$$\text{VaR}_{ML}(\alpha) = \kappa \cdot \text{VaR}_{t+1}(\alpha),$$

with $\kappa \in \{1 - b_1, 1 + b_2\}$. By the positive homogeneity of the original VaR, $\text{VaR}_{ML}(\alpha)$ therefore inherits the same property. Moreover, since the adjustment is monotonic and preserves the sign of $\text{VaR}_{t+1}(\alpha)$, subadditivity and translation invariance are unaffected. Hence, $\text{VaR}_{ML}(\alpha)$ retains the theoretical properties of the original Value-at-Risk. \square

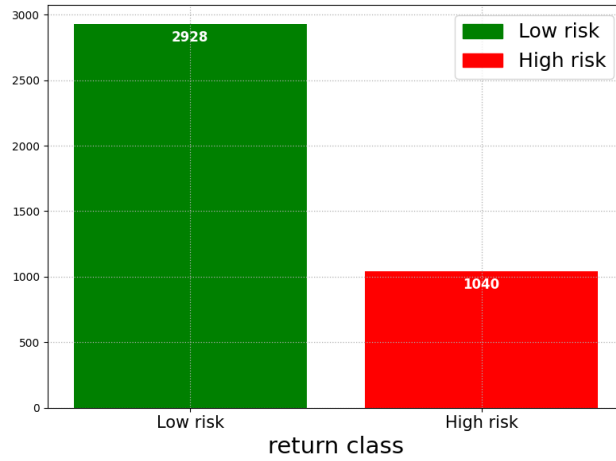


Figure 3: Proportion of different return classes

2.5 Machine Learning

Figure 3 illustrates the imbalanced class problem arising from the threshold-based binary classification of returns presented in Figure 2b. In this setting, the majority of returns are classified as low-risk, while the minority corresponding to high-risk events linked to Value-at-Risk (VaR) violations remains underrepresented. Traditional supervised learning models such as logistic regression (Dreiseitl and Ohno-Machado, 2002), Support Vector Machines (Vapnik, 1999; Tang et al., 2008) and neural network architectures including perceptrons, multilayer perceptrons (Rosenblatt, 1958; Murtagh, 1991), recurrent neural networks (Ampomah et al., 2020; Sunny et al., 2020), and temporal convolutional networks (Lea et al., 2016), tend to favor the majority class, thus reducing their effectiveness in detecting rare but crucial high-risk outcomes.

Several sampling strategies have been proposed to address this imbalance. Undersampling methods such as Edited Nearest Neighbors (ENN), Random Undersampling, and Tomek Links (Kotsiantis et al., 2006; Barandela et al., 2004; Elhassan and Aljurf, 2016; Zeng et al., 2016; Pereira et al., 2020) reduce the dominance of the majority class, but at the cost of discarding potentially informative observations, thereby impairing model robustness. In contrast, oversampling techniques such as SMOTE, Borderline-SMOTE, ADASYN, and Random Oversampling (Chawla et al., 2002; Han et al., 2005; Zhang and Li, 2014) artificially enrich the minority class, but risk overfitting, since synthetic instances may not capture the true underlying distribution.

Moreover, standard optimization objectives like mean squared error (MSE) or cross-entropy loss are dominated by the majority class, leading to weight updates that minimize overall error without improving minority class detection.

To evaluate models under such an imbalance, we employ a comprehensive set of performance metrics. Accuracy, precision, recall, and the F1 score, each capturing different trade-offs between type I and type II errors. However, these metrics remain sensitive to class imbalance, often overstating performance when the majority class dominates. To mitigate this bias, we additionally adopt the Geometric Mean (G-Mean), defined as

$$G\text{-Mean} = \sqrt{\text{Recall} \times \text{Specificity}},$$

which balances sensitivity to both minority-class detection (Recall) and majority-class recognition (Specificity). Unlike the F1-score, which emphasizes precision-recall trade-offs, the G-Mean penalizes classifiers that perform well in one class while neglecting the other, making it particularly suited to highly imbalanced financial data.

Given the shortcomings of sampling techniques and conventional metrics, we adopt the Double Deep Q-Network (DDQN) (Van Hasselt et al., 2016) as a reinforcement learning-based alternative. Unlike purely supervised models, DDQN learns adaptive policies through interaction with the environment, optimizing a reward function rather than a static loss. This enables a more effective handling of class imbalance by dynamically focusing on rare but high impact outcomes, offering a more robust framework for risk-sensitive classification and ultimately improving the accuracy of VaR estimation.

2.6 Reinforcement learning

Although supervised learning relies on labeled data to approximate a mapping between inputs and outputs, its performance deteriorates in settings characterized by severe class imbalance or sequential dependence. Reinforcement learning (RL) provides a fundamentally different paradigm by seeking to learn an optimal policy that maximizes cumulative rewards through interaction with a dynamic environment. Rather than minimizing prediction error, the agent operates in a trial-and-error framework: it selects actions, observes outcomes, and updates its strategy based on rewards, enabling adaptive learning in contexts where rules are uncertain or evolve over time.

Originally formalized by Sutton and Barto (1998), RL extends beyond the limitations of dynamic programming (Puterman, 2014), which requires complete knowledge of the environment and suffers from the ‘curse of dimensionality’ and beyond Monte Carlo approaches (Gilks et al., 1995), which fail to exploit temporal dependencies effectively. The standard framework is that of a Markov Decision Process (MDP) (White III and White, 1989), in which states, actions, and rewards are linked by probabilistic transitions. Central to this approach is the value function, which estimates expected long-term returns and is recursively defined by the Bellman equation. The agent–environment interaction underlying this MDP structure is illustrated in Figure 4, which highlights the sequential feedback loop that drives policy optimization.

The integration of deep learning into RL has led to powerful algorithms such as the Double Deep Q-Network (DDQN) (Van Hasselt et al., 2016) capable of scaling to high-dimensional and nonstationary environments. Using this framework, RL offers a flexible and robust alternative to supervised models, particularly in financial contexts characterized by volatility, structural breaks, and class imbalance. Its adaptive decision-making capacity makes it especially suitable for Value-at-Risk estimation, where capturing rare but high-impact events is essential for effective risk management.

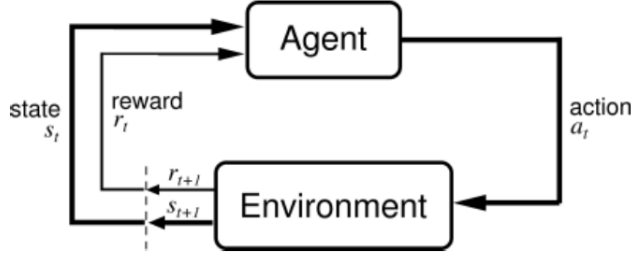


Figure 4: Agent-environment interaction model (Sutton and Barto, 1998)

Building on these principles, we adopt the Double Deep Q-Network (DDQN) framework, which combines the flexibility of reinforcement learning with the representational power of deep neural networks, providing an adaptive and robust approach to addressing the class imbalance and dynamic risk conditions inherent in Value-at-Risk estimation.

2.6.1 Markov Decision Process

To address the challenge of Value-at-Risk estimation under class imbalance, we formulate the problem as a Markov Decision Process (MDP). An MDP is defined by the tuple $\langle \mathcal{S}, \mathcal{A}, \mathcal{P}, \mathcal{R}, \gamma \rangle$, where each element corresponds to a key component of the sequential decision-making framework.

- States (\mathcal{S}): Each state $s_t \in \mathcal{S}$ represents the financial environment at time t , including the information needed to classify the return (e.g., recent volatility dynamics and lagged returns).
- Actions (\mathcal{A}): The agent chooses between two possible actions: $a_t \in 0, 1$, where 0 indicates a prediction of 'low risk' (majority class) and 1 indicates 'high risk' (minority class).
- State Transitions (\mathcal{P}): The transition function \mathcal{P} governs how the environment evolves after an action. In our context, transitions are deterministic in the sense that the next state s_{t+1} is determined by the sequence of observed returns, while the chosen action influences only the reward signal.
- Rewards (\mathcal{R}): The reward function evaluates the quality of the agent's classification and follows a design widely used in the reinforcement learning literature for unbalanced classification tasks (Firdous et al., 2023). In particular, the correct detection of rare but critical 'high-risk' events (true positives) is strongly rewarded, while missing such an event (false negative) incurs the most severe penalty. To correct for class imbalance, we incorporate a scaling factor $\rho \in (0, 1]$, defined as the ratio of minority to majority class sizes. This ensures that both classes contribute proportionally to the agent's learning process, a principle consistent with cost-sensitive reinforcement learning frameworks. The reward R_{t+1} can be defined as :

$$R_{t+1} = \begin{cases} +\rho & a_t \text{ is True Negative} \\ -\rho & a_t \text{ is False Negative} \\ +1 & a_t \text{ is True Positive} \\ -1 & a_t \text{ is False Positive} \end{cases} \quad (12)$$

Concretely:

- True Negative: $+\rho$ (moderate reward for correct classification of the majority class)
- False Negative: $-\rho$ (penalty weighted to reflect the rarity and severity of high-risk events)
- True Positive: $+1$ (successful detection of a critical event)
- False Positive: -1 (penalty to discourage unnecessary false alarms).
- Discount Factor (γ): Finally, $\gamma \in [0, 1]$ balances immediate and future rewards, ensuring that the agent optimizes long-term performance rather than short-sighted performance.

2.6.2 Policy and Value Functions

In reinforcement learning, a policy $\pi : \mathcal{S} \rightarrow \mathbb{A}$ defines the decision rule mapping each state $s_t \in \mathcal{S}$ to a probability distribution over possible actions. In our setting, the policy can be viewed as a classifier, where actions correspond to risk labels: $a \in \{0, 1\}$, with 0 denoting 'low risk' and 1 denoting 'high risk.' Formally,

$$\pi_t(a|s) = \mathbb{P}(a_t = a | s_t = s). \quad (13)$$

The agent's goal is to maximize the expected cumulative discounted reward, defined as:

$$G_t = \sum_{k=0}^{\infty} \gamma^k R_{t+k}, \quad (14)$$

where $\gamma \in [0, 1)$ is the discount factor that balances the importance of immediate versus future rewards.

The state value function in policy π measures the expected return starting from state s and then following policy π :

$$v_{\pi}(s) = \mathbb{E}_{\pi}[G_t | s_t = s]. \quad (15)$$

The optimal state-value function is then

$$v^*(s) = \max_{\pi} v_{\pi}(s), \quad \forall s \in \mathcal{S}. \quad (16)$$

Similarly, the action value function (or Q function) evaluates the expected return of taking action a in state s and thereafter following policy π :

$$Q_{\pi}(s, a) = \mathbb{E}_{\pi}[G_t | s_t = s, a_t = a]. \quad (17)$$

The optimal Q-function is

$$Q^*(s, a) = \max_{\pi} Q_{\pi}(s, a), \quad \forall s \in \mathcal{S}, a \in \mathbb{A}. \quad (18)$$

Using Bellman's optimality principle, the recursive form is expressed as follows:

$$Q^*(s, a) = \mathbb{E} \left[R_t + \gamma \max_{a'} Q^*(s_{t+1}, a') \mid s_t = s, a_t = a \right]. \quad (19)$$

This formalization, consistent with the applications in finance (Cui et al., 2023), allows the policy to dynamically adapt to signals. The agent gradually learns to classify high-risk states more accurately by associating state-action pairs with long-term returns, overcoming the limitations of static supervised learning in highly imbalanced financial data.

2.6.3 Double Deep Q-Network (DDQN)

Traditional Q-learning (Watkins, 1989) estimates the value of each state-action pair through iterative updates, but its reliance on tabular Q-tables makes it impractical in environments with large or continuous state spaces. The transition from Q-learning to Deep Q-Networks (DQN) addresses the curse of dimensionality inherent in tabular approaches. In DQN, the Q-function is approximated by a deep neural network parameterized by θ , yielding an estimate of the value of taking action a_t in state s_t . The target value combines the immediate reward with the discounted future return:

$$y_t^{DQN} = R_{t+1} + \gamma \max_{a_{t+1} \in \mathbb{A}} \hat{Q}_{\pi}(s_{t+1}, a_{t+1}; \theta^-), \quad (20)$$

where R_{t+1} reflects the reward associated with the classification at time $t+1$, γ is the discount factor, and θ^- denotes the weights of the target network, updated periodically to stabilize learning. The network parameters are optimized by minimizing the loss function:

$$\mathcal{L}^{DQN}(\theta) = \mathbb{E} \left[(y_t^{DQN} - Q_{\pi}(s_t, a_t; \theta))^2 \right]. \quad (21)$$

This loss represents the expected square difference between the predicted Q-value and the target y_t^{DQN} . In our classification context, minimizing $\mathcal{L}^{DQN}(\theta)$ ensures that the model better aligns its predictions (classifying 'Low risk' vs. 'High risk') with the true risk labels, especially rewarding correct detection of minority ('high-risk') cases. The replay buffer supplies mini-batches of past experiences, enabling balanced exposure to both classes despite data imbalance. Despite these improvements, standard DQNs often suffer from systematic overestimation of Q-values, leading to suboptimal policy selection. To mitigate this, the Double Deep Q-Network (DDQN) introduces two distinct networks: an evaluation network that selects actions and a target network that evaluates them. The update rule can be expressed compactly as

$$Q_\pi^{(i)}(s_t, a_t) \leftarrow (1 - \alpha)Q_\pi^{(i)}(s_t, a_t) + \alpha \left[R_{t+1} + \gamma \max_{a_{t+1} \in \mathbb{A}} Q_\pi^{(j)}(s_{t+1}, a_{t+1}) \right], \quad (22)$$

with $i \in \{1, 2\}$, $j = 3 - i$, and α the learning rate. Here, one network determines which action (classification) appears optimal, while the other provides the corresponding Q-value, reducing the upward bias of single-network estimation. The DDQN target value is then

$$y_t^{DDQN} = R_{t+1} + \gamma \max_{a_{t+1} \in \mathbb{A}} \hat{Q}_\pi \left(s_{t+1}, \arg \max_{a_{t+1} \in \mathbb{A}} Q_\pi(s_{t+1}, a_{t+1}; \theta); \theta^- \right). \quad (23)$$

Training proceeds by minimizing the corresponding DDQN loss function,

$$\mathcal{L}^{DDQN}(\theta) = \mathbb{E} \left[(y_t^{DDQN} - Q_\pi(s_t, a_t; \theta))^2 \right]. \quad (24)$$

In practice, this loss penalizes incorrect risk predictions more heavily for the minority class ('high risk') due to the reward structure, ensuring that the model gradually prioritizes the accurate classification of rare but critical events. By combining experience replay with the alternating update of evaluation and target networks, DDQN achieves both stability and robustness, directly improving the detection of Value-at-Risk violations.

3 Empirical results

3.1 Data and Features Selection

We evaluated our models using the Euro Stoxx 50 index, which represents the 50 largest capitalizations in the eurozone. The dataset, obtained from Yahoo¹ Finance, covers the period from September 1, 2008, to March 13, 2025. Although the Euro Stoxx 50 is a natural benchmark for European equity markets, it also presents important challenges for predictive modeling. Because the index undergoes periodic revisions, with constituents added or removed to reflect evolving market conditions, the direct use of its lagged components introduces discontinuities and structural breaks. This dynamic would require continuous recalibration of models, reducing both their robustness and their generalizability.

To address this issue, we adopt a more stable framework that emphasizes variables that capture broad market and macroeconomic dynamics rather than firm-specific fluctuations. The explanatory set therefore integrates major eurozone equity indices such as the CAC 40 and DAX, which provide information on regional and sectoral diversification. Key currency pairs including EUR/USD and EUR/GBP are incorporated to reflect the role of exchange rates in European competitiveness and capital flows. In addition, technical indicators such as Simple and Exponential Moving Averages and the Relative Strength Index are included, as they translate price dynamics into signals that can anticipate short-term market reversals. Finally, conditional volatility forecasts derived from GARCH and GJR-GARCH specifications are employed to account for the heteroskedastic and asymmetric nature of financial returns.

¹<https://fr.finance.yahoo.com/>

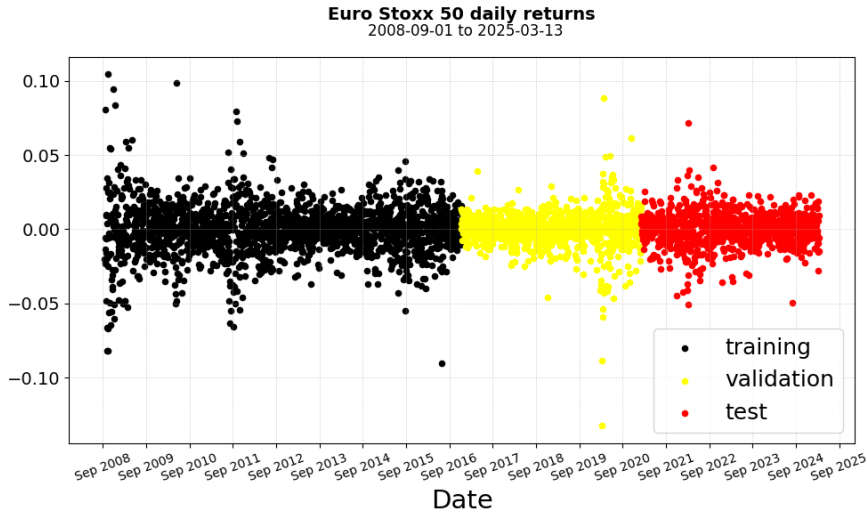


Figure 5: Data set splitting

To ensure a rigorous and unbiased evaluation of the predictive framework, the data set is chronologically divided into three distinct sub-samples: training, validation, and test (Figure 5). The training sample, which constitutes the bulk of the data, is used to estimate the model parameters by learning the relationships between the explanatory variables and the target risk classification. The validation set serves to fine-tune the hyperparameters and prevent overfitting, thereby enhancing the generalizability of the model. The final test sample is reserved exclusively for out-of-sample evaluation, providing a realistic assessment of predictive performance on unseen data and ensuring that the reported results are not driven by in-sample optimization.

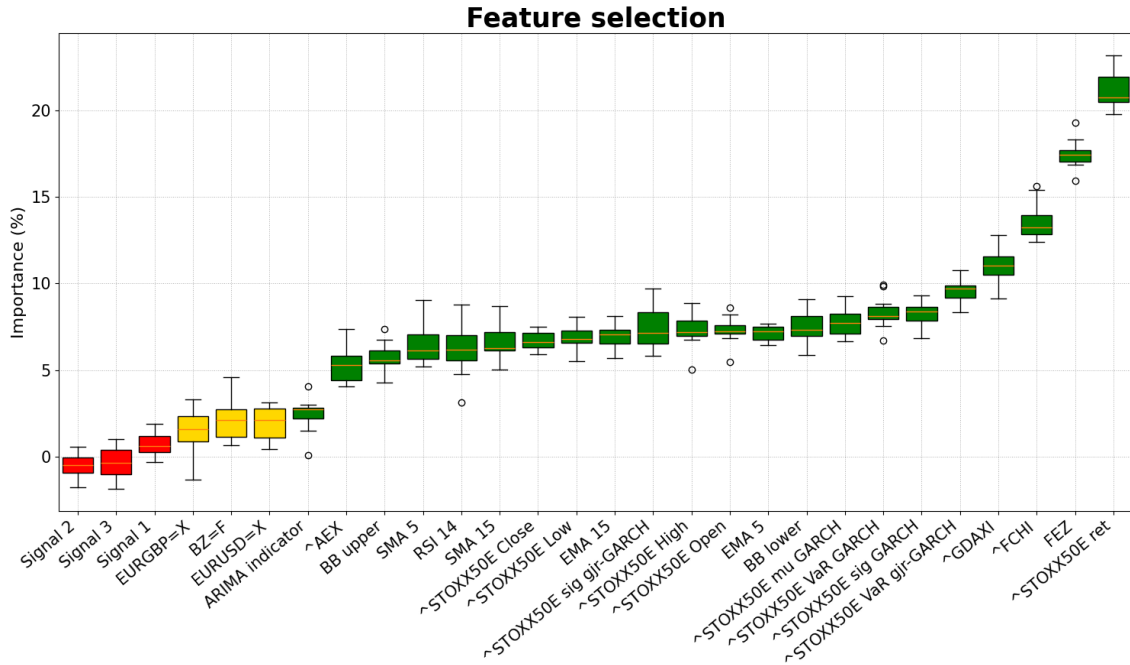


Figure 6: Features selection

The selection of features is performed using the Boruta algorithm (Kursa and Rudnicki, 2010; Kursa et al., 2010), a wrapper method particularly suited for high-dimensional nonlinear financial datasets. This approach identifies explanatory variables with a statistically significant contribution to predictive accuracy. Figure 6 presents the ranking of the selected features. Economically, the results are intuitive: The lagged returns of the Euro Stoxx 50 account for roughly 20% of the explanatory power, consistent with the notion that the past information is rapidly incorporated by the

European equity markets. The CAC 40 contributes approximately 13%, reflecting the importance of sectoral and regional effects. The volatility forecasts explain the difference between 8% and 10%, confirming the central role of expected volatility in risk formation. Interestingly, the FEZ ETF, which closely tracks the Euro Stoxx 50, adds an additional 17%, suggesting that liquidity effects and intra-day adjustments convey information not fully embedded in the raw index. In contrast, exchange rates such as EUR/USD and EUR/GBP display weaker explanatory power, consistent with their indirect influence on daily equity risk. Technical indicators also provide additional, though more limited, information, particularly in detecting momentum shifts.

The descriptive statistics for the returns, explanatory characteristics, strategy positions, and qualitative variables are reported in Tables 1, 2, 3 and 4. Table 1 confirms that the return distributions are stationary but non-normal, exhibiting skewness and excess kurtosis. These findings underscore the prevalence of fat tails and justify the reliance on nonlinear predictive models. While stationarity ensures the validity of econometric inference, the presence of non-normality highlights the need to capture extreme events. Table 2 further reveals a significant heterogeneity in the scale of the explanatory variables, motivating the use of Min-Max normalization as a pre-processing step. This transformation improves numerical stability and accelerates convergence in hybrid econometric-machine learning frameworks, according to recommendations in the literature (Han et al., 2005). Tables 3 and 4 provide additional information on the signals generated by trading strategies and the forecasts derived from the ARIMA and hybrid ARIMA-ANN models, both of which enrich the information set for subsequent classification tasks.

Assets	Mean (%)	Std (%)	Skewness	Kurtosis	Min	Max	ADF	Jarque-Bera
EURUSD=X	-0.007	0.724	0.782	113.692	-0.143	0.160	-12.606	2136941.801
EURGBP=X	0.001	0.598	0.166	62.569	-0.111	0.110	-33.930	647122.057
BZ=F	-0.006	2.440	-0.606	13.962	-0.280	0.212	-63.680	32465.986
FEZ	0.019	1.741	-0.409	9.130	-0.133	0.162	-11.813	13887.933
[^] FCHI	0.017	1.409	-0.188	8.671	-0.131	0.106	-21.735	12451.577
[^] GDAXI	0.034	1.399	-0.087	8.742	-0.131	0.116	-20.348	12637.285
[^] AEX	0.022	1.311	-0.327	9.672	-0.114	0.100	-12.401	15532.029
[^] STOXX50E	0.014	1.429	-0.245	7.909	-0.132	0.104	-21.293	10379.093

Table 1: Descriptive statistics for returns

Features	Mean	Std	Min	Max
[^] STOXX50E Close	3346.722	706.846	1809.980	5540.690
[^] STOXX50E High	3370.447	705.616	1823.250	5568.190
[^] STOXX50E Low	3321.543	707.570	1765.490	5506.570
[^] STOXX50E Open	3346.747	706.032	1812.780	5531.530
BB upper	3469.825	694.591	2139.143	5597.252
BB lower	3213.444	701.508	1670.766	5324.596
EMA 5	3345.631	703.870	1854.835	5495.911
EMA 15	3342.931	696.996	1954.528	5455.968
SMA 5	3345.639	704.382	1857.532	5490.536
SMA 15	3342.891	698.354	1925.779	5481.875
RSI 14	52.626	11.333	10.728	79.894
[^] STOXX50E μ GARCH	-0.000	0.002	-0.049	0.024
[^] STOXX50E sig GARCH	0.013	0.006	0.005	0.057
[^] STOXX50E sig gjr-GARCH	0.013	0.006	0.005	0.057
[^] STOXX50E VaR GARCH	-0.021	0.011	-0.138	-0.006
[^] STOXX50E VaR gjr-GARCH	-0.021	0.011	-0.138	-0.006

Table 2: Descriptive statistics for features

Strategy	Sell	Stay	Buy
Simple Moving Average Cross	3681	143	143
Exponential Moving Average Cros	3631	168	168
Relative Strength Index	3662	165	140

Table 3: Descriptive statistics for positions in different trading strategies

Variables	Low risk	High risk
ARIMA indicator	2951	1016
risk level	2928	1039

Table 4: Descriptive statistics of qualitative variables

3.2 Classification under Imbalanced Data

The target variable is the binary risk level, defined in Section 2.3 and visualized in Figure 7. In training, validation and test sets, low-risk observations represent about 70%, with high-risk accounting for 30%. Although not extreme, this imbalance poses a challenge: Standard classifiers tend to overexcite the majority class, impairing the detection of high-risk periods, precisely those with the greatest economic costs. To address this, we compared under-sampling and over-sampling strategies. Undersampling reduced imbalance, but at the cost of lost information. In contrast, the ADASYN algorithm (He et al., 2008) effectively generated synthetic minority samples, improving the detection of high-risk states with minimal bias, albeit at the cost of a longer training.

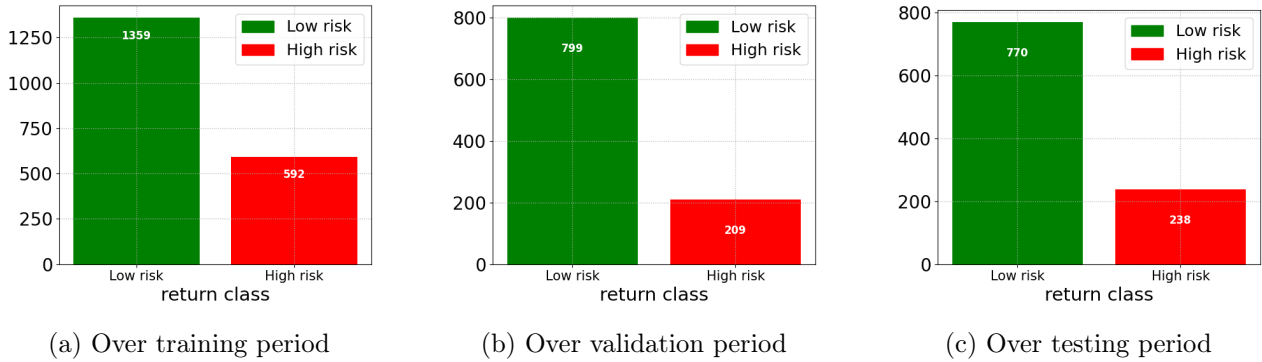


Figure 7: Barplot of different risk levels

We benchmarked multiple models: Logistic regression (LR), Support Vector Machines (SVM), Single-Layer Perceptron (ANN), Multi-Layer Perceptron (MLP), Temporal Convolutional Network (TCN), and our Double Deep Q-Network (DDQN). All supervised methods were combined with ADASYN for fairness. Model performance is assessed not only by accuracy, but also by F1 score, recall, precision, and G-mean, as accuracy alone may be misleading in imbalanced contexts. Economically, these metrics align with the risk manager’s priorities: Recall reflects the ability to capture high-risk episodes; precision limits costly false alarms; and G-Mean balances the two, avoiding asymmetric errors. Table 5 reports the results. Reinforcement Learning achieved the strongest performance: accuracies of 83.5% (validation) and 79.4% (test), F1 scores greater than 0.66 and recall values of 0.574 (validation) and 0.54 (test), the highest among all models. G-Mean scores (0.735 validation, 0.714 test) confirm balanced detection between classes. TCN also performed well, but consistently behind RL.

The economic importance is clear: the superior recall of the RL framework minimizes undetected high-risk returns, reducing the likelihood of underestimated losses, and enabling more proactive risk mitigation strategies.

Metric	LR	SVM	ANN	MLP	TCN	RL
Accuracy	0.616	0.639	0.618	0.719	0.788	0.835
F1-score	0.375	0.370	0.368	0.499	0.587	0.668
Recall	0.283	0.290	0.280	0.396	0.492	0.574
Precision	0.555	0.512	0.536	0.675	0.727	0.799
G-Mean	0.489	0.494	0.485	0.596	0.672	0.735

Metric	LR	SVM	ANN	MLP	TCN	RL
Accuracy	0.514	0.524	0.530	0.678	0.720	0.794
F1-score	0.412	0.431	0.398	0.527	0.595	0.661
Recall	0.289	0.300	0.285	0.403	0.452	0.540
Precision	0.723	0.765	0.660	0.761	0.870	0.853
G-Mean	0.492	0.508	0.485	0.602	0.653	0.714

(a) On validation sample

(b) On testing sample

Table 5: Model performance

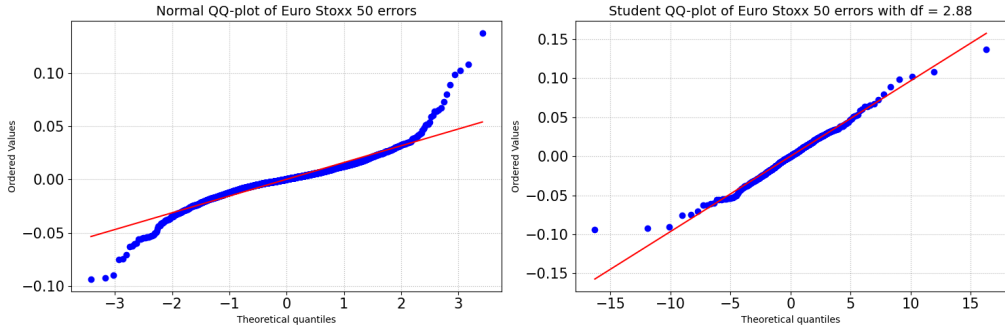


Figure 8: QQ-plot of Euro Stoxx 50 errors distribution

3.3 Evaluation of the Classification-Adjusted Value-at-Risk

After determining the accuracy of the risk classification, we now evaluate the Classification Adjusted Value-at-Risk (VaR) framework defined in Equation (11). This approach scales traditional GARCH or GJR-GARCH VaR estimates up or down depending on predicted risk level, using adjustment parameters b_1 and b_2 . To capture conditional volatility dynamics, we use both the GARCH and GJR-GARCH specifications. Given empirical evidence of fat tails (Table 1, Figure 8), we adopt the Student distribution t , which better reflects the heavy-tailed nature of the Euro Stoxx 50 returns. Tables 6–8 summarize the results. As shown in Table 6, the RL-adjusted VaR significantly reduces skewness and kurtosis in predictive distributions. For example, the $VaR_{RL}^{\text{GARCH}}(\alpha = 5\%)$ model achieves a skewness of -2.048 and a kurtosis of 8.613 in the test sample, far closer to empirical distributions than conventional models. The results of the backtest confirm the robustness. The Christoffersen conditional coverage test (Table 7) indicates that RL-adjusted VaR models pass through validation and test samples, for both 5% and 1% levels, unlike conventional models that are systematically rejected. The Kupiec test (Table 8) further validates the adequacy of the violation frequencies, with the RL models showing no systematic bias.

From an economic point of view, these results demonstrate that RL-adjusted VaR not only achieves statistical validity but also enhances risk management decisions. By reducing false alarms (overestimated risk) and missed warnings (underestimated risk), it enables more efficient capital allocation, ensures regulatory compliance, and improves early warning capacity during volatile periods.

Model	Version	Min	Median	Mean	Std	Skewness	Kurtosis	Max
$VaR^{\text{GARCH}}(\alpha = 5\%)$	Original	-0.136	-0.013	-0.016	0.012	-5.101	35.265	-0.005
	TCN	-0.129	-0.010	-0.014	0.012	-4.747	31.630	-0.004
	RL	-0.138	-0.010	-0.014	0.011	-4.929	36.258	-0.004
$VaR^{\text{GJR}}(\alpha = 5\%)$	Original	-0.148	-0.013	-0.016	0.012	-5.436	40.562	-0.005
	TCN	-0.141	-0.010	-0.014	0.012	-4.891	35.097	-0.004
	RL	-0.137	-0.011	-0.014	0.012	-5.092	38.121	-0.004
$VaR^{\text{GARCH}}(\alpha = 1\%)$	Original	-0.194	-0.022	-0.027	0.018	-4.481	27.036	-0.011
	TCN	-0.190	-0.017	-0.024	0.018	-4.280	25.984	-0.008
	RL	-0.205	-0.017	-0.023	0.018	-4.402	29.152	-0.008
$VaR^{\text{GJR}}(\alpha = 1\%)$	Original	-0.215	-0.021	-0.027	0.019	-4.772	31.483	-0.010
	TCN	-0.210	-0.017	-0.024	0.019	-4.350	28.127	-0.007
	RL	-0.204	-0.018	-0.023	0.019	-4.534	30.670	-0.007

(a) On validation sample

Model	Version	Min	Median	Mean	Std	Skewness	Kurtosis	Max
$VaR^{\text{GARCH}}(\alpha = 5\%)$	Original	-0.059	-0.015	-0.017	0.005	-2.588	13.231	-0.008
	TCN	-0.071	-0.014	-0.015	0.007	-2.118	9.694	-0.005
	RL	-0.069	-0.013	-0.015	0.006	-2.048	8.613	-0.005
$VaR^{\text{GJR}}(\alpha = 5\%)$	Original	-0.054	-0.015	-0.017	0.006	-2.033	6.564	-0.007
	TCN	-0.065	-0.014	-0.016	0.008	-1.759	5.142	-0.005
	RL	-0.057	-0.013	-0.015	0.007	-1.757	4.732	-0.005
$VaR^{\text{GARCH}}(\alpha = 1\%)$	Original	-0.097	-0.026	-0.028	0.008	-2.485	11.885	-0.014
	TCN	-0.116	-0.024	-0.026	0.011	-2.031	8.645	-0.010
	RL	-0.116	-0.022	-0.025	0.010	-2.058	8.783	-0.010
$VaR^{\text{GJR}}(\alpha = 1\%)$	Original	-0.083	-0.026	-0.028	0.009	-1.997	6.015	-0.013
	TCN	-0.100	-0.023	-0.026	0.013	-1.723	4.754	-0.010
	RL	-0.096	-0.022	-0.025	0.011	-1.773	4.874	-0.010

(b) On testing sample

Table 6: Statistical indicators for VaR models

Model	Version	Expected violations	Actual violations	Test statistic	Test critical value	Test p-value	Decision
$VaR^{\text{GARCH}}(\alpha = 5\%)$	Original	50	73	9.4259	3.8414	0.0368	Reject H_0
	TCN	50	72	8.6521	3.8414	0.0032	Reject H_0
	RL	50	52	0.0075	3.8414	0.9310	Accept H_0
$VaR^{\text{GJR}}(\alpha = 5\%)$	Original	50	68	5.8597	3.8414	0.0154	Reject H_0
	TCN	50	72	8.6521	3.8414	0.0032	Reject H_0
	RL	50	53	0.4234	3.8414	0.5002	Accept H_0
$VaR^{\text{GARCH}}(\alpha = 1\%)$	Original	10	19	6.3276	3.8414	0.0118	Reject H_0
	TCN	10	25	13.9951	3.8414	0.0002	Reject H_0
	RL	10	12	0.8288	3.8414	0.3856	Accept H_0
$VaR^{\text{GJR}}(\alpha = 1\%)$	Original	10	19	6.3276	3.8414	0.0118	Reject H_0
	TCN	10	24	13.9951	3.8414	0.0002	Reject H_0
	RL	10	11	0.0824	3.8414	0.7741	Accept H_0

(a) On validation sample

Model	Version	Expected violations	Actual violations	Test statistic	Test critical value	Test p-value	Decision
$VaR^{\text{GARCH}}(\alpha = 5\%)$	Original	50	64	3.5722	3.8414	0.0587	Accept H_0
	TCN	50	47	0.2467	3.8414	0.6193	Accept H_0
	RL	50	52	0.0075	3.8414	0.9310	Accept H_0
$VaR^{\text{GJR}}(\alpha = 5\%)$	Original	50	64	3.5722	3.8414	0.0587	Accept H_0
	TCN	50	52	0.0529	3.8414	0.8180	Accept H_0
	RL	50	55	0.4297	3.8414	0.5121	Accept H_0
$VaR^{\text{GARCH}}(\alpha = 1\%)$	Original	10	13	0.7828	3.8414	0.3762	Accept H_0
	TCN	10	13	0.7828	3.8414	0.3762	Accept H_0
	RL	10	11	0.0823	3.8414	0.7741	Accept H_0
$VaR^{\text{GJR}}(\alpha = 1\%)$	Original	10	12	0.3481	3.8414	0.5551	Accept H_0
	TCN	10	10	0.0006	3.8414	0.9797	Accept H_0
	RL	10	11	0.0824	3.8414	0.7741	Accept H_0

(b) On testing sample

Table 7: Christoffersen test of VaR models

Model	Version	Test statistic	Test critical value	Test p-value	Decision
$VaR^{GARCH}(\alpha = 5\%)$	Original	13.4338	5.9914	0.0012	Reject H_0
	TCN	10.2577	5.9914	0.0059	Reject H_0
	RL	7.6298	5.9914	0.0320	Reject H_0
$VaR^{GJR}(\alpha = 5\%)$	Original	5.9509	5.9914	0.0510	Accept H_0
	TCN	10.2577	5.9914	0.0059	Reject H_0
	RL	5.9593	5.9914	0.0510	Accept H_0
$VaR^{GARCH}(\alpha = 1\%)$	Original	7.0584	5.9914	0.02932	Reject H_0
	TCN	16.0076	5.9914	0.0003	Reject H_0
	RL	4.5624	5.9914	0.1021	Accept H_0
$VaR^{GJR}(\alpha = 1\%)$	Original	0.9907	5.9914	0.6093	Accept H_0
	TCN	15.1671	5.9914	0.0005	Reject H_0
	RL	3.4969	5.9914	0.1740	Accept H_0
$VaR^{GARCH}(\alpha = 5\%)$	Original	4.5021	5.9914	0.1052	Accept H_0
	TCN	0.2660	5.9914	0.8754	Accept H_0
	RL	1.3806	5.9914	0.5014	Accept H_0
$VaR^{GJR}(\alpha = 5\%)$	Original	3.5735	5.9914	0.1675	Accept H_0
	TCN	0.2643	5.9914	0.8761	Accept H_0
	RL	2.3948	5.9914	0.3019	Accept H_0
$VaR^{GARCH}(\alpha = 1\%)$	Original	1.1229	5.9914	0.5703	Accept H_0
	TCN	1.1229	5.9914	0.5703	Accept H_0
	RL	4.5624	5.9914	0.1021	Accept H_0
$VaR^{GJR}(\alpha = 1\%)$	Original	0.6376	5.9914	0.7270	Accept H_0
	TCN	0.2012	5.9914	0.9042	Accept H_0
	RL	0.3253	5.9914	0.8498	Accept H_0

(a) On validation sample

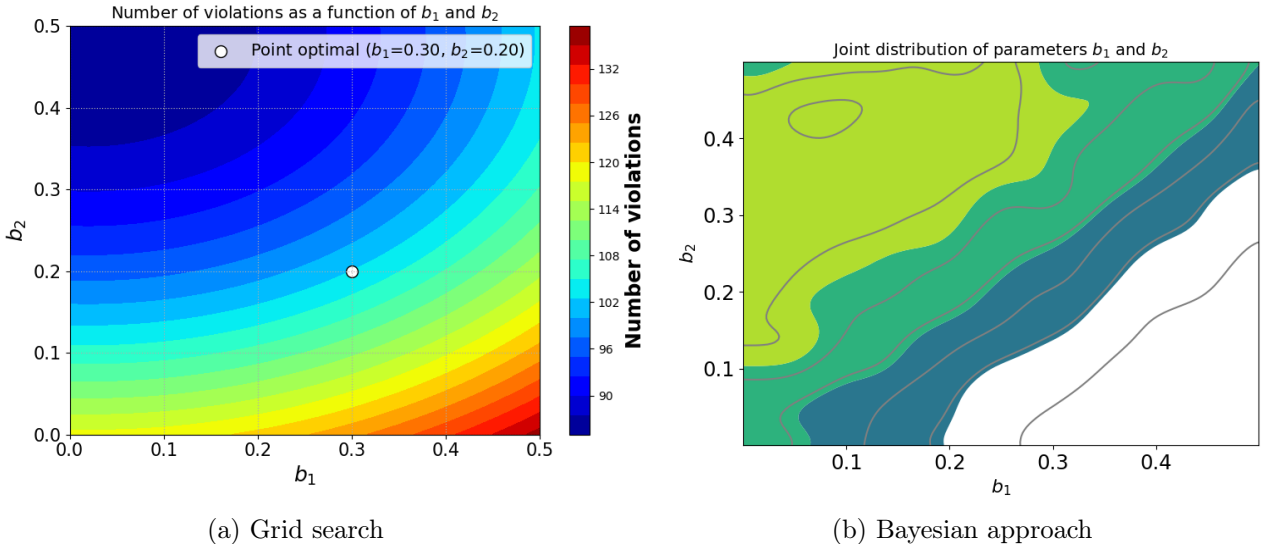
(b) On testing sample

Table 8: Kupiec test of VaR models

4 Discussions

4.1 Calibration of Classification-Adjusted Value-at-Risk parameters

To ensure the statistical credibility and practical relevance of the proposed Classification-Adjusted Value-at-Risk (VaR) model, we calibrate the adjustment parameters (b_1, b_2) using two complementary methodologies. The first relies on a rolling-window cross-validation procedure designed to account for the temporal dependence inherent in financial time series. The second adopts a fully Bayesian perspective through Markov Chain Monte Carlo (MCMC) estimation, allowing a probabilistic characterization of parameter uncertainty. The cross-validation approach explores a grid of (b_1, b_2) combinations and evaluates their performance in terms of the number of VaR violations across validation windows. As illustrated in Figure 9a, the violation surface shows a clear minimum, indicating that the pair $(b_1 = 0.30, b_2 = 0.20)$ produces the lowest number of exceedances. This empirical optimum ensures that the adjusted VaR provides sufficient coverage while preserving the independence of violations over time, as further confirmed by serial independence tests. Economically, this adjustment corresponds to reducing VaR by 30% in periods predicted as low risk and increasing it by 20% in high risk states. Such magnitudes reflect a well-balanced trade-off: they partially correct for potential underestimation without disproportionately relying on the predictive power of the classification model. To avoid overreactive adjustments, the grid search was limited to values below 0.5.

Figure 9: Calibration of parameters b_1 and b_2

To further substantiate the robustness of these parameter choices, we estimate the joint posterior distribution of (b_1, b_2) using a Bayesian MCMC sampling scheme. Figure 9b shows the resulting posterior density, with darker regions denoting higher credibility. The empirical optimum $(0.30, 0.20)$ lies within the high-density region, reinforcing its plausibility under a statistical inference framework.

Interestingly, the posterior contours reveal a negative correlation between the parameters: stronger downward adjustments in low-risk periods (higher b_1) must be counterbalanced by more conservative upward adjustments in high-risk states (lower b_2) to maintain consistent coverage. This interdependence highlights the importance of calibrating the adjustment mechanism as a coherent system rather than in isolation. Taken together, the cross-validation and Bayesian analyses provide a rigorous and mutually reinforcing justification for the chosen adjustment parameters.

Although cross-validation ensures empirical performance in a realistic, time-dependent setting, Bayesian inference offers a probabilistic understanding of parameter uncertainty. This dual calibration strategy improves the credibility, transparency and robustness of the proposed VaR adjustment mechanism, providing a principled foundation for practical deployment in financial risk management.

4.2 Robustness Analysis via Extreme Value Theory

Beyond traditional backtesting procedures such as the Kupiec and Christoffersen tests, it is essential to examine the robustness of our Classification Adjusted Value-at-Risk (VaR) model in the tails of the return distribution. In this regard, Extreme Value Theory (EVT) offers a rigorous statistical foundation to evaluate the model's ability to capture rare but financially devastating events. According to the Pickands–Balkema–de Haan theorem, the distribution of losses exceeding a high threshold asymptotically follows a Generalized Pareto Distribution (GPD), making it a natural candidate for tail modeling in financial risk. To operationalize this framework, we extract the exceedances over the adjusted VaR thresholds $\text{VaR}_{\text{ML}}(\alpha)$ and fit a GPD to these residual losses. The adequacy of the fitted model is assessed using the Kolmogorov–Smirnov (KS) test, where the null hypothesis posits that the observed exceedances are drawn from a GPD. A p-value exceeding 5% implies that the null hypothesis cannot be rejected, suggesting consistency between empirical tail behavior and the fitted extreme value model.

Table C1 reports the location of the estimated GPD parameters $\hat{\mu}$, scale $\hat{\beta}$, and shape $\hat{\xi}$ alongside the KS test statistics and p values for both validation and testing samples, across the different model configurations (Original, TCN and RL). The results reveal a systematic pattern: For all configurations, the KS p-values consistently exceed the 5% threshold, confirming the statistical validity of the GPD fit across the board. A particularly noteworthy observation concerns the validation sample, which chronologically aligns with the Covid-19 crisis period, a phase marked by high volatility, structural breaks, and extreme tail risk.

During this period, several RL-adjusted models, such as $\text{VaR}_{\text{RL}}^{\text{GARCH}}(5\%)$ and $\text{VaR}_{\text{RL}}^{\text{GJR}}(1\%)$, produced estimated shape parameters $\hat{\xi} > 1$. This is economically significant: a shape parameter above one implies an infinite second moment of the loss distribution, consistent with the breakdown of conventional risk assumptions in systemic events. Such heavy-tailed behavior reinforces the need to use conservative and adaptive risk measures capable of capturing non-linear tail dynamics.

From a risk management point of view, these findings provide strong empirical support for the classification-adjusted VaR framework. Not only do the chosen adjustment parameters ($b_1 = 0.30, b_2 = 0.20$) ensure accurate coverage in the backtesting, but they also preserve consistency with EVT-based tail modeling. Dual validation in terms of unconditional violations and conditional tail distributions substantiates the robustness of our proposed approach under real-world stress conditions. Finally, the robustness of the adjusted VaR in both validation and testing samples, as indicated by p-values ranging from 0.06 to 0.99, confirms that the model does not underestimate risk in critical periods. This is crucial for both regulatory compliance (e.g., under Basel III recommendations) and internal risk governance, where reliable tail estimation informs capital adequacy planning and strategic hedging decisions.

4.3 Comparative Performance of VaR Adjustments

The integration of classification-adjusted Value-at-Risk (VaR) models, particularly those relying on reinforcement learning (RL) and temporal convolutional networks (TCN), leads to marked improvements in both statistical performance and economic efficiency relative to conventional volatility-based models. These gains are most evident when examining the model's ability to control violation rates, adapt to changing risk regimes, optimize capital allocation, and maintain robustness in structurally unstable market environments. From a statistical perspective, Reinforcement Learning–driven VaR models exhibit superior calibration properties. As evidenced by the Kupiec and Christoffersen back-test results (Tables 7 and 8), the RL approach maintains coverage levels closely aligned with theoretical expectations while satisfying the independence assumption of violations, a condition systematically rejected for GARCH and GJR-GARCH models at conventional significance levels. The absence of temporal clustering in violations further underscores the improved ability of the RL framework to capture the stochastic structure of returns.

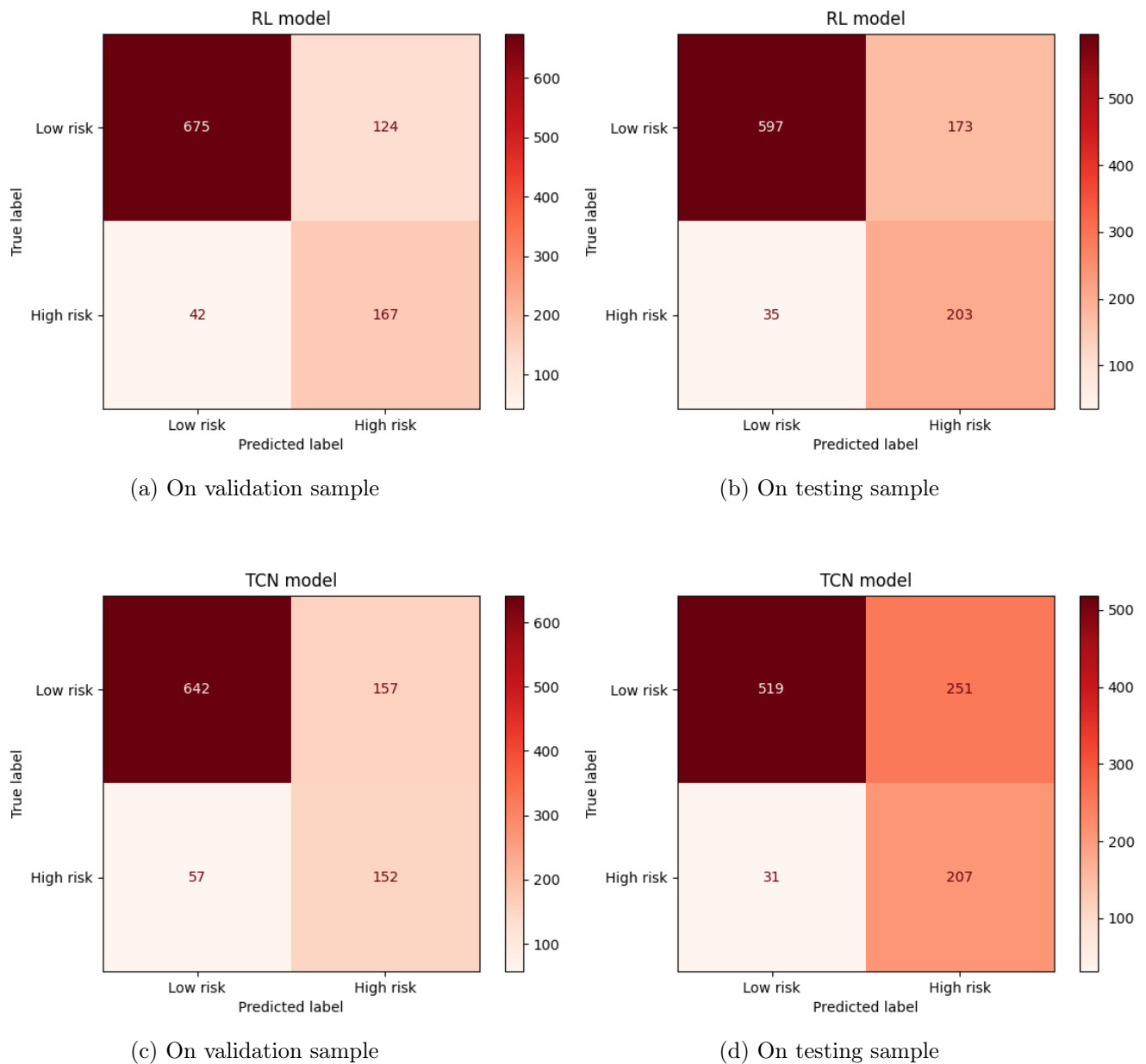


Figure 10: Confusion matrices for RL and TCN models

These findings are further supported by the aggregated violation counts reported in Table 9, where the RL-adjusted VaR consistently reports fewer exceedances than both GARCH-type and TCN models, particularly at the 5% risk level. The nonparametric Wilcoxon rank-sum test (Table 10) confirms the statistical significance of this difference, with a p-value of 0.0039 indicating robust outperformance in tail coverage. This improved statistical validity is not merely a technical refinement; it has direct consequences for portfolio protection during high-volatility episodes.

The source of this enhanced control lies in the accurate classification of the underlying risk states. Figures 10 and 11 reveal that the RL model achieves high precision in distinguishing between low-risk and high-risk regimes. In the validation and test samples, it correctly identifies 675 and 597 low-risk periods, respectively, allowing substantial downward adjustments to the VaR during tranquil market phases. In parallel, the TCN model proves more effective in detecting high-risk episodes, with 167 and 203 accurate classifications across the two samples, prompting timely increases in capital buffers. The alignment between these classifications and real-world market events, such as the COVID-19 pandemic or post-pandemic geopolitical shocks, highlights the capacity of these models to dynamically recalibrate risk estimates in response to structural breaks.

Beyond predictive accuracy, the economic implications of these adjustments are nontrivial. Efficient risk management requires that VaR models not only safeguard against losses but also avoid excessive capital conservatism. In this regard, Figures 13 and 14 illustrate that the RL and TCN models tend to produce less negative VaR estimates than GJR-GARCH, achieving similar levels of coverage with lower implicit capital requirements. This distributional shift is statistically validated by the Mann–Whitney test (Table 11), which shows that the RL model produces significantly higher (i.e. less conservative) VaR medians across the thresholds 1% and 5%, under both validation and test conditions. The ability to reduce capital charges without compromising regulatory compliance constitutes a substantial operational advantage, particularly in capital-constrained environments.

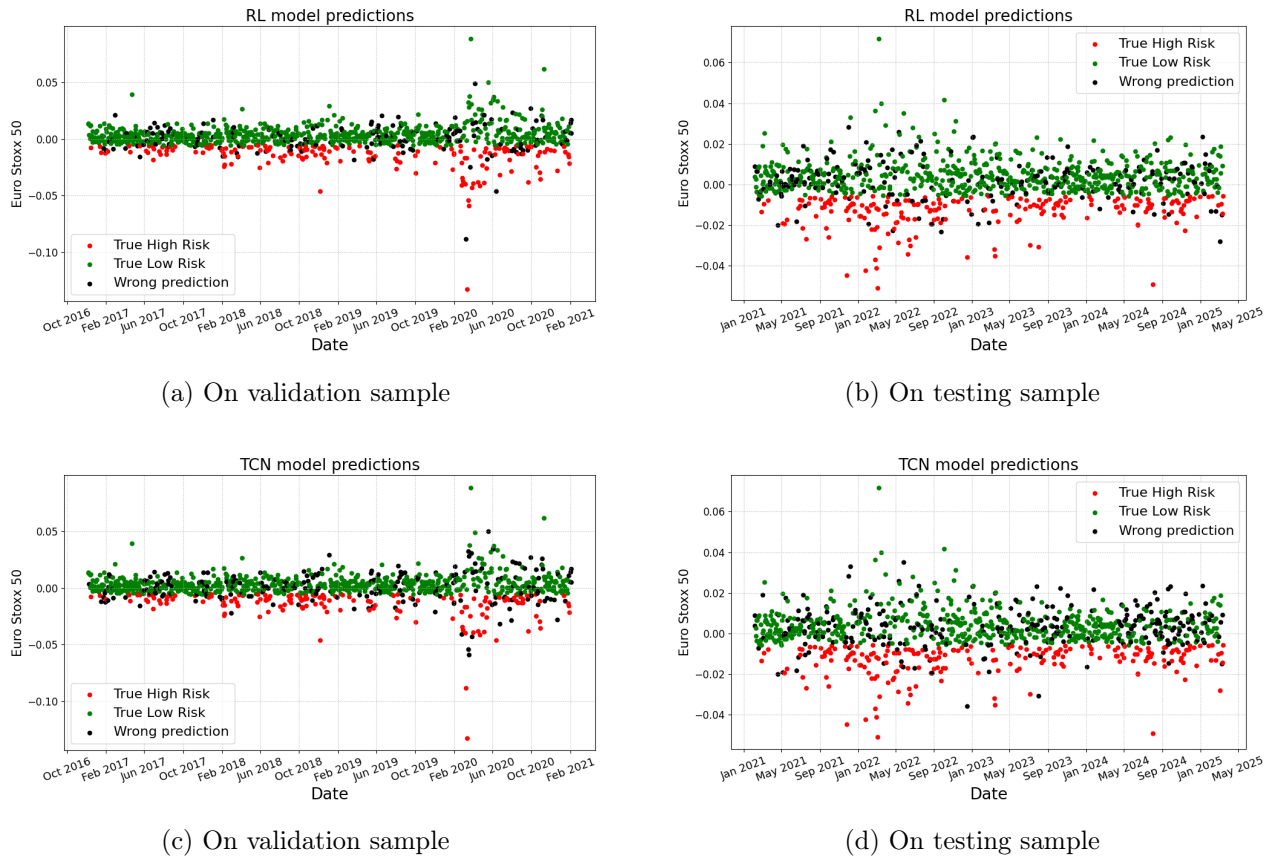


Figure 11: Prediction of risk levels

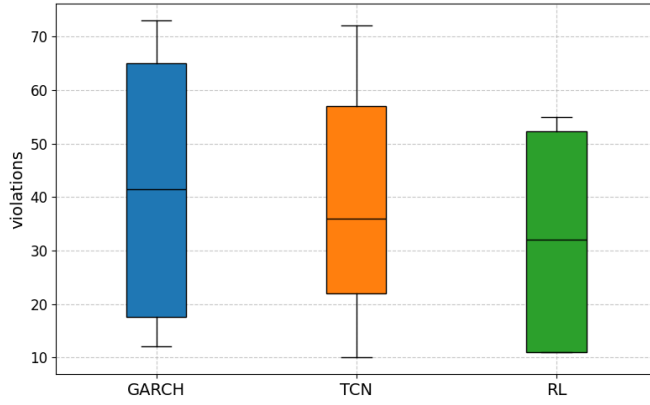


Figure 12: Boxplots of VaR violation

Sample	Model	GARCH	TCN	RL
validation	GARCH 95%	73	72	52
	GJR 95%	68	72	53
	GARCH 99%	19	25	12
	GJR 99%	13	13	11
testing	GARCH 95%	64	47	52
	GJR 95%	64	52	55
	GARCH 99%	13	13	11
	GJR 99%	12	10	11

Table 9: VaR violation

However, the performance of the TCN model is more nuanced. Although it outperforms traditional benchmarks in the test sample, it exhibits greater sensitivity during periods of extreme volatility, leading to a higher frequency of violations. This relative instability limits its effectiveness under highly turbulent conditions, where the adaptive structure of the RL model is more robust. Importantly, these performance gains are achieved under challenging empirical conditions.

The two analyzed subsamples span prolonged episodes of financial instability, including the aftermath of Brexit, the COVID-19 pandemic, rising inflation, and geopolitical turmoil following the Russia–Ukraine conflict. Such environments violate many of the assumptions underlying traditional econometric models, particularly stationarity and linearity, and underscore the need for models capable of learning from non-standard and evolving dynamics. In this context, the dynamic adjustment of VaR thresholds via classification-informed modulation parameterized by b_1 and b_2 emerges as a central innovation. It enables the model to scale risk estimates in real time, expanding the buffer in periods of increased uncertainty while relaxing constraints during stable market conditions. This adaptability is especially valuable for institutions that want to align capital reserves with prevailing risk profiles and report risk measures that are both responsive and explainable.

Test hypotheses		Test indicators	TCN vs GARCH	RL vs GARCH	TCN vs RL
$H_0 : \mu_1 = \mu_2$	vs $H_1 : \mu_1 < \mu_2$	Test statistic P-value	12 0.3997	0.0 0.0039	8 0.0976

Table 10: Equality test for VaR violation means

α	Ind stat	GARCH		GJR-GARCH	
		TCN	RL	TCN	RL
5%	statistic	243568	228198	241408	235833
	p-value	0.1236	0.0136	0.08212	0.02308
1%	statistic	252784	238663	241376	236536
	p-value	0.4362	0.04572	0.08159	0.0436

(a) On validation sample

α	Ind stat	GARCH		GJR-GARCH	
		TCN	RL	TCN	RL
5%	statistic	234618	226652	220530	235833
	p-value	0.01678	0.0014	0.0001	0.02308
1%	statistic	237250	236431	238642	238250
	p-value	0.03284	0.02685	0.0455	0.04159

(b) On testing sample

Table 11: Mann-Whitney test between distributions of $\text{VaR}_{t+1}(\alpha)$ and $\text{VaR}_{ML}(\alpha)$

4.4 Regulatory Implications and Methodological Limitations

The financial crisis of 2007–2009 revealed critical weaknesses in conventional Value-at-Risk (VaR) models, particularly their inability to capture rare but catastrophic events. This motivated a series of reforms by the Basel Committee on Banking Supervision ([Supervision, 2011, 2012](#); [on Banking Supervision, 2017](#)), culminating in the replacement of VaR by a more robust and coherent risk measure: the Expected Shortfall (ES).

Unlike VaR, which only considers a quantile of the return distribution, ES evaluates the conditional expectation of losses beyond the VaR threshold. Formally, the Expected Shortfall at confidence level α is defined as:

$$ES_{t+1}(\alpha) = \mathbb{E}[r_{t+1} \mid r_{t+1} < \text{VaR}_{t+1}(\alpha)]$$

where r_{t+1} denotes the future return for the next time period.

This makes clear that VaR remains a fundamental component in the regulatory risk architecture, as its estimation directly underpins the calculation of ES. In this context, improving the quality of VaR estimates, especially under non-normal and volatile conditions, is of both theoretical and operational importance. Our approach contributes to this objective by proposing a hybrid architecture based on Temporal Convolutional Networks (TCN) and deep reinforcement learning (DRL), which offers enhanced flexibility in capturing nonlinear dynamics and regime shifts. These models leverage long-memory structures and adaptive learning mechanisms, making them distinct from traditional GARCH-type frameworks that rely on rigid parametric assumptions.

To address regulatory concerns about model transparency, we have incorporated a variable selection step based on the Boruta algorithm, which identifies statistically significant features for classification. This contributes to the interpretability of the system by clarifying the informational basis upon which the risk regime classifier operates. In addition, the risk classification step itself, implemented prior to VaR adjustment, can be interpreted as a structural decision rule separating high- and low-risk periods, supported by confusion matrices and predictive performance metrics.

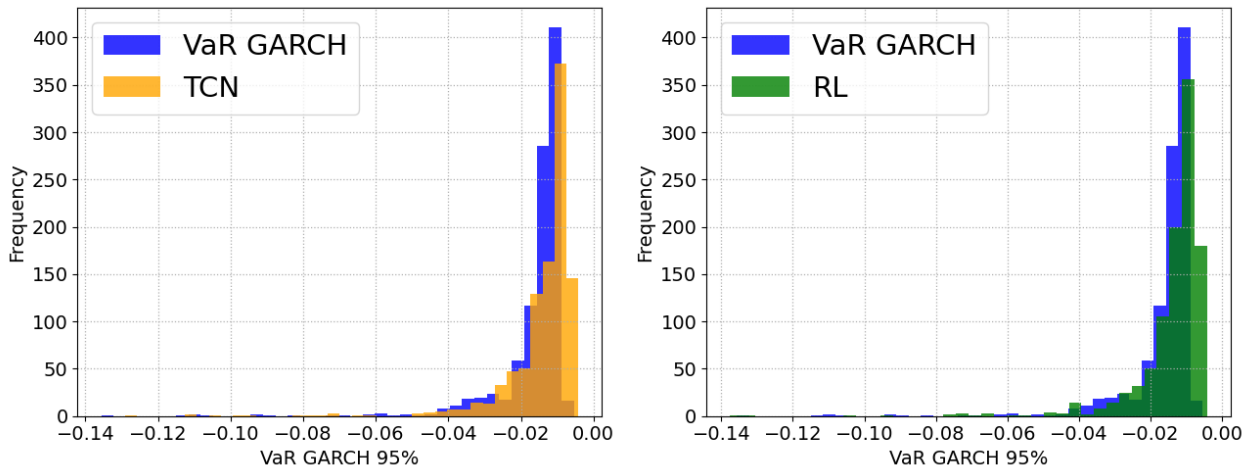


Figure 13: Comparison of VaR distributions with a GJR-GARCH volatility process on the validation sample

However, we recognize that further interpretation of our DRL model remains a major challenge. Deep neural network decisions are inherently "black boxes," which is problematic in critical domains such as financial risk management (Guidotti et al., 2018; Rudin, 2019). To address this lack of transparency, we could explore post-hoc explanation tools such as SHAP (SHapley Additive ExPlanations) (Lundberg and Lee, 2017) or LIME (Local Interpretable Model-Agnostic Explanations) (Ribeiro et al., 2016). Although these techniques apply to all types of model, a particularly promising avenue would be to train a surrogate model, such as a random forest or XGBoost classifier to approximate the behavior of our DRL agent. By analyzing the decision rules of this interpretable surrogate, we could derive an intuitive representation of the underlying logic that governs the risk adjustment process. Beyond interpretability, the practical implementation of such models poses significant computational challenges. DRL and TCN architectures require careful calibration, high-dimensional optimization, and nontrivial training infrastructure. The neural network architectures and hyperparameters are fully specified in the appendix D.

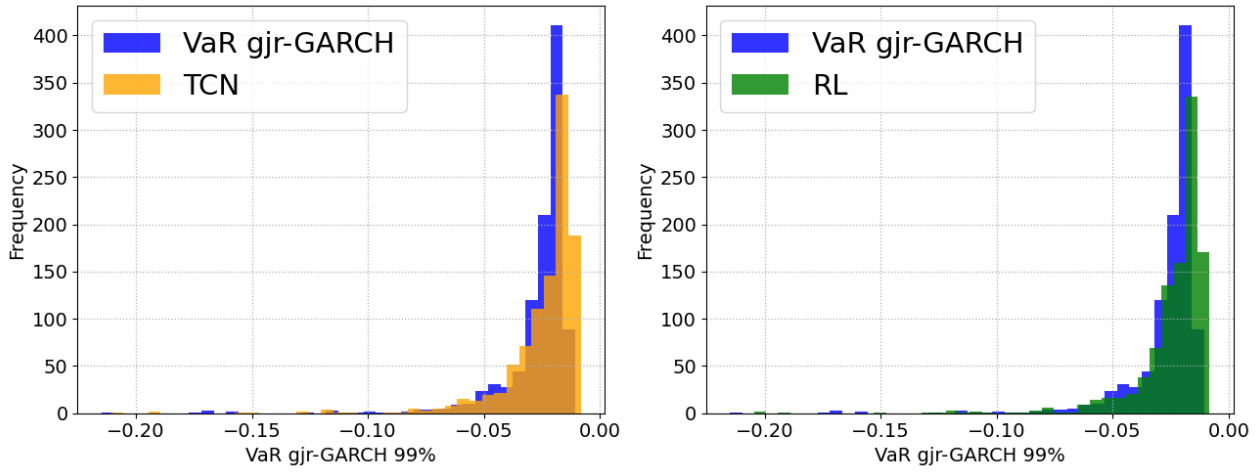


Figure 14: Comparison of VaR distributions with a GJR-GARCH volatility process on the testing sample

These demands may hinder their adoption by institutions that lack the technical capacity or regulatory confidence to implement black-box models. However, our empirical results show that these architectures significantly reduce VaR violations while maintaining statistical validity under standard backtesting procedures, including the Kupiec and Christoffersen tests. This performance, combined with their dynamic adaptability, suggests strong potential in active capital management frameworks. In summation, while deep learning-based approaches open promising perspectives for risk estimation and capital efficiency, their successful adoption in regulatory contexts will depend on continued efforts to enhance their interpretability, transparency, and reproducibility. This includes developing companion tools that explain the logic of risk classifications, quantifying uncertainty in model output, and establishing clear audit trails. These developments are essential to align machine learning innovations with the standards of prudential supervision and the broader expectations of financial governance.

5 Conclusion

This paper introduces a novel framework for Value-at-Risk (VaR) estimation that combines predictive classification with dynamic adjustment mechanisms, enabling more responsive and capital-efficient risk measurement. By reformulating the challenge of market risk forecasting into an imbalanced classification problem addressed through a Double Deep Q-Network (DDQN) reinforcement learning algorithm, our method captures non-nonlinearity, structural changes, and the asymmetric nature of financial return distributions.

Empirical analysis of the Euro Stoxx 50 index, covering more than 16 years of data and several episodes of market stress, demonstrates that the proposed classification-adjusted VaR model significantly outperforms traditional volatility-based approaches. Reduce both the number and temporal clustering of violations, passes standard backtesting procedures (Kupiec and Christoffersen), and aligns with the tail behavior predicted by Extreme Value Theory. From an economic standpoint, the model enables more efficient capital allocation by providing less conservative VaR estimates without compromising regulatory coverage.

For practitioners and policymakers, the following strategic takeaways emerge:

- Risk-level classification enhances tail risk management: Adjusting VaR thresholds according to predicted low- and high-risk periods enables closer alignment of capital buffers with prevailing market conditions.
- Reinforcement learning enables adaptive forecasting: Unlike static models, the agent continuously updates its classification strategy in response to changing patterns in return dynamics.

- Compliance with regulatory standards is preserved: The methodology remains compatible with the expected shortfall framework and satisfies key statistical requirements, ensuring relevance in Basel III contexts.
- Capital efficiency and risk sensitivity can coexist: The approach reduces unnecessary capital charges during stable periods while enhancing protection during volatile episodes.

However, several limitations should be acknowledged. Its implementation involves non-trivial computational complexity, sensitivity to hyperparameters, and reduced interpretability compared to classical models. Although this limitation is mitigated through Boruta-based feature selection and structural performance evaluation through classification metrics, more work is needed to improve transparency, especially through the development of surrogate model-based explanation tools to enhance decision auditability.

Compliance with Ethical Standards

Declaration of Competing Interest

All authors declare that they have no conflicts of interest.

Ethical approval:

This article does not contain any studies with human participants or animals performed by any of the authors.

References

H. Alostad and H. Davulcu. Directional prediction of stock prices using breaking news on twitter. In *Web Intelligence*, volume 15, pages 1–17. IOS Press, 2017.

E. K. Ampomah, Z. Qin, and G. Nyame. Evaluation of tree-based ensemble machine learning models in predicting stock price direction of movement. *Information*, 11(6):332, 2020.

R. Barandela, R. M. Valdovinos, J. S. Sánchez, and F. J. Ferri. The imbalanced training sample problem: Under or over sampling? In *Structural, Syntactic, and Statistical Pattern Recognition: Joint IAPR International Workshops, SSPR 2004 and SPR 2004, Lisbon, Portugal, August 18-20, 2004. Proceedings*, pages 806–814. Springer, 2004.

T. Bollerslev. Generalized autoregressive conditional heteroskedasticity. *Journal of econometrics*, 31(3):307–327, 1986.

N. V. Chawla, K. W. Bowyer, L. O. Hall, and W. P. Kegelmeyer. Smote: synthetic minority oversampling technique. *Journal of artificial intelligence research*, 16:321–357, 2002.

J. Chung and Y. Hong. Model-free evaluation of directional predictability in foreign exchange markets. *Journal of Applied Econometrics*, 22(5):855–889, 2007.

T. Cui, S. Ding, H. Jin, and Y. Zhang. Portfolio constructions in cryptocurrency market: A cvar-based deep reinforcement learning approach. *Economic Modelling*, 119:106078, 2023.

S. Dreiseitl and L. Ohno-Machado. Logistic regression and artificial neural network classification models: a methodology review. *Journal of biomedical informatics*, 35(5-6):352–359, 2002.

T. Elhassan and M. Aljurf. Classification of imbalance data using Tomek link (t-link) combined with random under-sampling (rus) as a data reduction method. *Global J Technol Optim S*, 1:2016, 2016.

T. Fawcett and F. Provost. Adaptive fraud detection. *Data mining and knowledge discovery*, 1(3):291–316, 1997.

N. Firdous, N. M. U. Din, and A. Assad. An imbalanced classification approach for establishment of cause-effect relationship between heart-failure and pulmonary embolism using deep reinforcement learning. *Engineering Applications of Artificial Intelligence*, 126:107004, 2023.

W. R. Gilks, S. Richardson, and D. Spiegelhalter. *Markov chain Monte Carlo in practice*. CRC press, 1995.

L. R. Glosten, R. Jagannathan, and D. E. Runkle. On the relation between the expected value and the volatility of the nominal excess return on stocks. *The journal of finance*, 48(5):1779–1801, 1993.

I. Goodfellow, Y. Bengio, A. Courville, and Y. Bengio. *Deep learning*, volume 1. MIT press Cambridge, 2016.

R. Guidotti, A. Monreale, S. Ruggieri, F. Turini, F. Giannotti, and D. Pedreschi. A survey of methods for explaining black box models. *ACM computing surveys (CSUR)*, 51(5):1–42, 2018.

H. Han, W.-Y. Wang, and B.-H. Mao. Borderline-smote: a new over-sampling method in imbalanced data sets learning. In *International conference on intelligent computing*, pages 878–887. Springer, 2005.

H. He, Y. Bai, E. A. Garcia, and S. Li. Adasyn: Adaptive synthetic sampling approach for imbalanced learning. In *2008 IEEE international joint conference on neural networks (IEEE world congress on computational intelligence)*, pages 1322–1328. Ieee, 2008.

A. Kanas. Neural network linear forecasts for stock returns. *International Journal of Finance & Economics*, 6(3):245–254, 2001.

S. Kotsiantis, D. Kanellopoulos, P. Pintelas, et al. Handling imbalanced datasets: A review. *GESTS international transactions on computer science and engineering*, 30(1):25–36, 2006.

M. B. Kursa and W. R. Rudnicki. Feature selection with the boruta package. *Journal of statistical software*, 36:1–13, 2010.

M. B. Kursa, A. Jankowski, and W. R. Rudnicki. Boruta—a system for feature selection. *Fundamenta Informaticae*, 101(4):271–285, 2010.

C. Lea, R. Vidal, A. Reiter, and G. D. Hager. Temporal convolutional networks: A unified approach to action segmentation. In *Computer Vision–ECCV 2016 Workshops: Amsterdam, The Netherlands, October 8–10 and 15–16, 2016, Proceedings, Part III 14*, pages 47–54. Springer, 2016.

O. Linton and Y.-J. Whang. The quantilogram: With an application to evaluating directional predictability. *Journal of Econometrics*, 141(1):250–282, 2007.

S. M. Lundberg and S.-I. Lee. A unified approach to interpreting model predictions. *Advances in neural information processing systems*, 30, 2017.

V. Mnih, K. Kavukcuoglu, D. Silver, A. Graves, I. Antonoglou, D. Wierstra, and M. Riedmiller. Playing atari with deep reinforcement learning. *arXiv preprint arXiv:1312.5602*, 2013.

T. Morimura, M. Sugiyama, H. Kashima, H. Hachiya, and T. Tanaka. Parametric return density estimation for reinforcement learning. *arXiv preprint arXiv:1203.3497*, 2012.

F. Murtagh. Multilayer perceptrons for classification and regression. *Neurocomputing*, 2(5-6):183–197, 1991.

L. Nevasalmi. Forecasting multinomial stock returns using machine learning methods. *The Journal of Finance and Data Science*, 6:86–106, 2020.

E. Noorani, C. N. Mavridis, and J. S. Baras. Risk-sensitive reinforcement learning with exponential criteria. *IEEE Transactions on Cybernetics*, 2025.

H. Nyberg. Forecasting the direction of the us stock market with dynamic binary probit models. *International Journal of Forecasting*, 27(2):561–578, 2011.

B. C. on Banking Supervision. Basel iii: Finalising post-crisis reforms. *Bank for International Settlements*, 2017.

R. M. Pereira, Y. M. Costa, and C. N. Silla Jr. Mltl: A multi-label approach for the tomek link undersampling algorithm. *Neurocomputing*, 383:95–105, 2020.

F. Pokou, J. Sadefo Kamdem, and F. Benhmad. Hybridization of arima with learning models for forecasting of stock market time series. *Computational Economics*, 63(4):1349–1399, 2024.

F. V. M. Pokou. *Une contribution sur l’allocation ou la prévision d’actifs d’un portefeuille*. PhD thesis, Université de Montpellier, 2022.

M. L. Puterman. *Markov decision processes: discrete stochastic dynamic programming*. John Wiley & Sons, 2014.

M. T. Ribeiro, S. Singh, and C. Guestrin. " why should i trust you?" explaining the predictions of any classifier. In *Proceedings of the 22nd ACM SIGKDD international conference on knowledge discovery and data mining*, pages 1135–1144, 2016.

F. Rosenblatt. The perceptron: a probabilistic model for information storage and organization in the brain. *Psychological review*, 65(6):386, 1958.

C. Rudin. Stop explaining black box machine learning models for high stakes decisions and use interpretable models instead. *Nature machine intelligence*, 1(5):206–215, 2019.

S. Stanko and K. Macek. Risk-averse distributional reinforcement learning: A cvar optimization approach. In *IJCCI*, pages 412–423, 2019.

M. A. I. Sunny, M. M. S. Maswood, and A. G. Alharbi. Deep learning-based stock price prediction using lstm and bi-directional lstm model. In *2020 2nd novel intelligent and leading emerging sciences conference (NILES)*, pages 87–92. IEEE, 2020.

B. Supervision. Basel committee on banking supervision. *Principles for Sound Liquidity Risk Management and Supervision (September 2008)*, 2011.

B. Supervision. Basel committee on banking supervision. 2012.

R. Sutton and A. Barto. Reinforcement learning: An introduction. *IEEE Transactions on Neural Networks*, 9(5):1054–1054, 1998.

Y. Tang, Y.-Q. Zhang, N. V. Chawla, and S. Krasser. Svms modeling for highly imbalanced classification. *IEEE Transactions on Systems, Man, and Cybernetics, Part B (Cybernetics)*, 39(1):281–288, 2008.

A. Tealab. Time series forecasting using artificial neural networks methodologies: A systematic review. *Future Computing and Informatics Journal*, 3(2):334–340, 2018.

I. Tomek. Two modifications of cnn. 1976.

H. Van Hasselt, A. Guez, and D. Silver. Deep reinforcement learning with double q-learning. In *Proceedings of the AAAI conference on artificial intelligence*, volume 30, 2016.

V. Vapnik. *The nature of statistical learning theory*. Springer science & business media, 1999.

C. J. C. H. Watkins. Learning from delayed rewards. 1989.

C. C. White III and D. J. White. Markov decision processes. *European Journal of Operational Research*, 39(1):1–16, 1989.

D. L. Wilson. Asymptotic properties of nearest neighbor rules using edited data. *IEEE Transactions on Systems, Man, and Cybernetics*, (3):408–421, 2007.

H. Yang, X.-Y. Liu, S. Zhong, and A. Walid. Deep reinforcement learning for automated stock trading: An ensemble strategy. In *Proceedings of the first ACM international conference on AI in finance*, pages 1–8, 2020.

C. Ying, X. Zhou, H. Su, D. Yan, N. Chen, and J. Zhu. Towards safe reinforcement learning via constraining conditional value-at-risk. *arXiv preprint arXiv:2206.04436*, 2022.

M. Zeng, B. Zou, F. Wei, X. Liu, and L. Wang. Effective prediction of three common diseases by combining smote with Tomek links technique for imbalanced medical data. In *2016 IEEE International Conference of Online Analysis and Computing Science (ICOACS)*, pages 225–228. IEEE, 2016.

G. P. Zhang. Time series forecasting using a hybrid arima and neural network model. *Neurocomputing*, 50:159–175, 2003.

H. Zhang and M. Li. Two-sampling: A random walk over-sampling approach to imbalanced data classification. *Information Fusion*, 20:99–116, 2014.

Q. Zhang, S. Leng, X. Ma, Q. Liu, X. Wang, B. Liang, Y. Liu, and J. Yang. Cvar-constrained policy optimization for safe reinforcement learning. *IEEE transactions on neural networks and learning systems*, 36(1):830–841, 2024.

A Selected features

nº	Asset	ID	Informations
1	AEX	$^{\wedge}$ AEX	Index
2	CAC 40	$^{\wedge}$ FCHI	Index
3	DAX	$^{\wedge}$ GDAXI	Index
4	Euro Stoxx 50	$^{\wedge}$ STOXX50E	Index
5	Brent Crude Oil Last Day	BZ=F	Commodity
6	EURO/USD	EURUSD=X	Currency
7	EURO/GBP	EURGBP=X	Currency
8	SPDR EURO STOXX 50 ETF	FEZ	ETF
9	Bollinger Bands	BB upper & BB lower	Technical trading indicator
10	Relative Strength Index	RSI 14	Technical trading indicator
11	Standard Moving Average	SMA 5 & SMA 15	Technical trading indicator
12	Exponentially Weighted Moving Average	EMA 5 & EMA 15	Technical trading indicator
13	Forecasting returns using GARCH model	$^{\wedge}$ STOXX50E mu GARCH	Econometric indicators
14	Forecasting volatility using GARCH model	$^{\wedge}$ STOXX50E sig GARCH	Econometric indicators
15	Forecasting volatility using GJR6GARCH model	$^{\wedge}$ STOXX50E sig gjr-GARCH	Econometric indicators
16	Forecasting VaR using GARCH model	$^{\wedge}$ STOXX50E VaR GARCH	Econometric indicators
17	Forecasting VaR using GJR-GARCH model	$^{\wedge}$ STOXX50E VaR gjr-GARCH	Econometric indicators
18	SMA strategy trading positions	Signal 1	Technical trading indicator
19	EMA strategy trading positions	Signal 2	Technical trading indicator
20	BB strategy trading positions	Signal 3	Technical trading indicator
21	Forecasting risk level of returns with ARIMA model	ARIMA indicator	Class prediction

Table A1: Selected features

B Confusion matrices

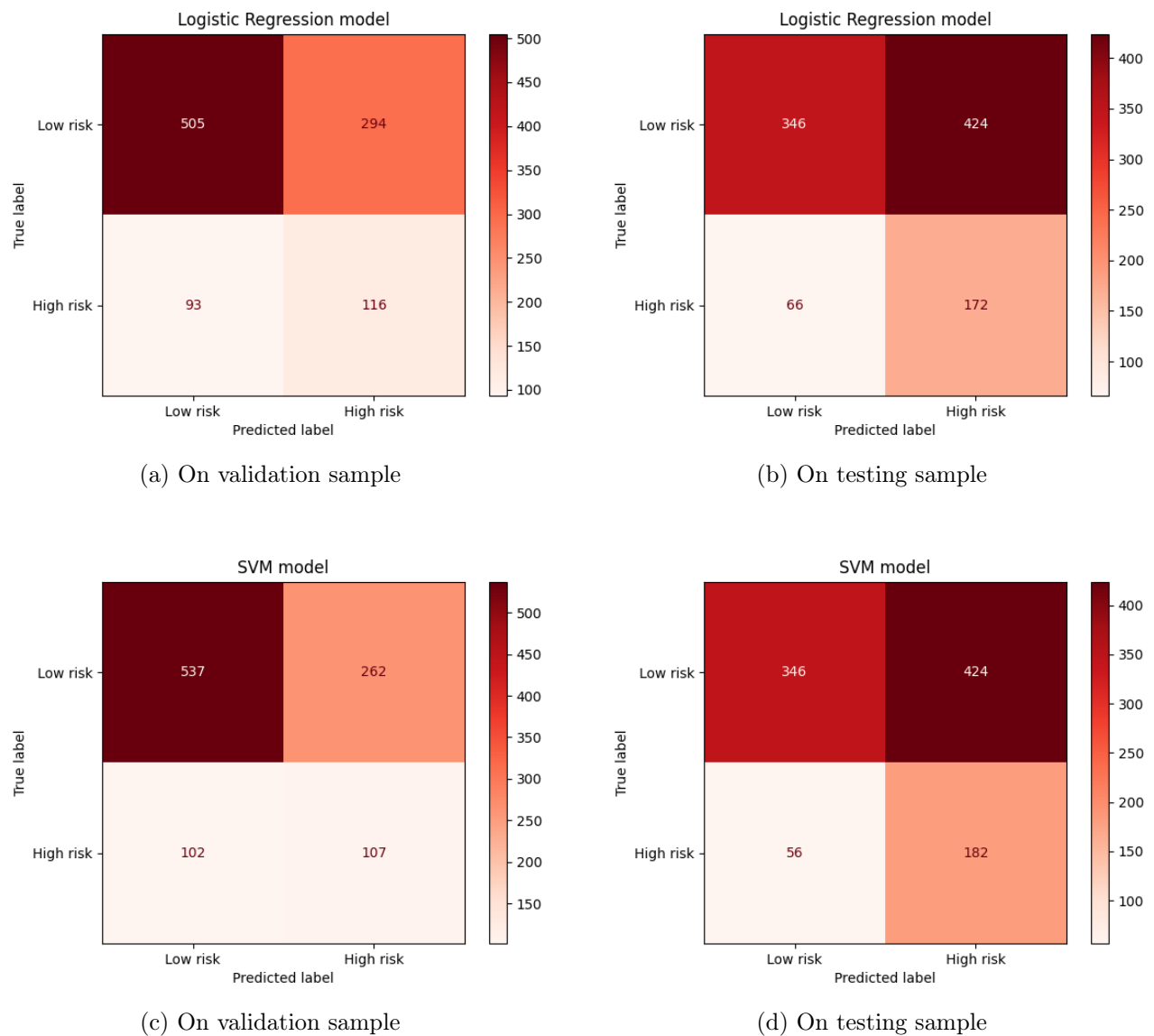


Figure B1: Confusion matrices for learning models

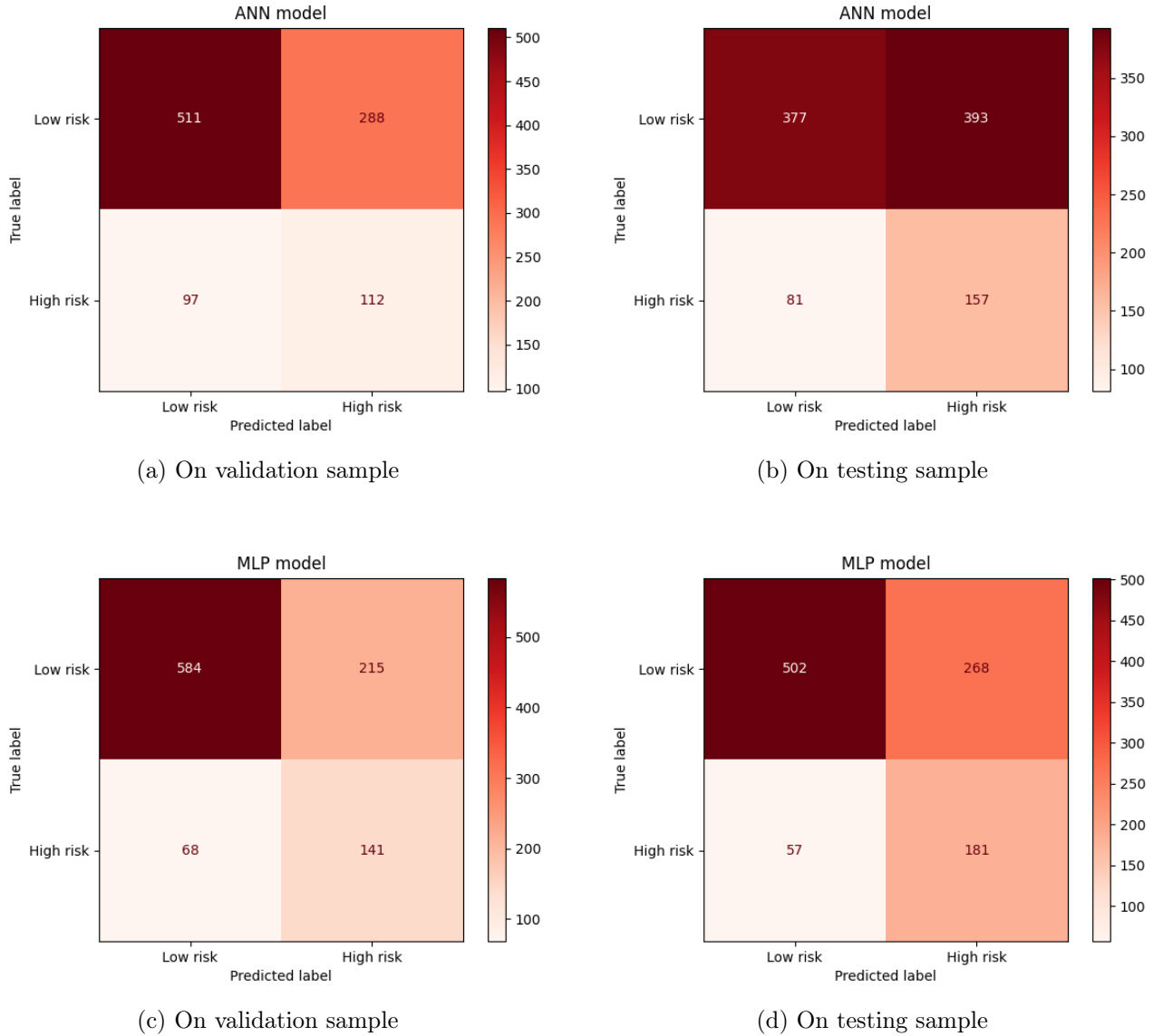


Figure B2: Confusion matrices for learning models

C VaR robustness tests

Model	Version	GPD parameters			Kolmogorov-Smirnov test	
		$\hat{\mu}$	$\hat{\beta}$	$\hat{\xi}$	stat	p-value
$VaR^{GARCH}(\alpha = 5\%)$	Original	0.0000	0.0067	0.2474	0.0973	0.4647
	TCN	0.0001	0.0035	1.4108	0.1555	0.0669
	RL	0.0002	0.0025	1.4020	0.1553	0.0641
$VaR^{GJR}(\alpha = 5\%)$	Original	0.0002	0.0044	1.3963	0.1847	0.0167
	TCN	0.0001	0.0047	0.4501	0.0677	0.8690
	RL	0.0001	0.0047	0.3549	0.0878	0.6394
$VaR^{GARCH}(\alpha = 1\%)$	Original	0.0000	0.0059	0.5109	0.1404	0.7988
	TCN	0.0006	0.0025	1.3735	0.1343	0.7082
	RL	0.0006	0.0032	1.3734	0.1736	0.6234
$VaR^{GJR}(\alpha = 1\%)$	Original	0.0002	0.0034	1.3992	0.1464	0.7577
	TCN	0.0009	0.0025	1.4937	0.1554	0.5559
	RL	0.0009	0.0024	1.2674	0.1314	0.9120

Model	Version	GPD parameters			Kolmogorov-Smirnov test	
		$\hat{\mu}$	$\hat{\beta}$	$\hat{\xi}$	stat	p-value
$VaR^{GARCH}(\alpha = 5\%)$	Original	0.0000	0.0049	0.4709	0.0719	0.8714
	TCN	0.0002	0.0040	1.4046	0.1627	0.1484
	RL	0.0005	0.0043	1.2900	0.1781	0.0691
$VaR^{GJR}(\alpha = 5\%)$	Original	0.0000	0.0047	0.3958	0.0458	0.9984
	TCN	0.0001	0.0046	0.3762	0.1020	0.6144
	RL	0.0006	0.0029	1.3873	0.1503	0.1505
$VaR^{GARCH}(\alpha = 1\%)$	Original	0.0004	0.0033	1.2981	0.1658	0.8120
	TCN	0.0001	0.0060	0.4435	0.1412	0.9258
	RL	0.0001	0.0056	0.4367	0.1378	0.9668
$VaR^{GJR}(\alpha = 1\%)$	Original	0.0001	0.0047	1.4028	0.2144	0.5678
	TCN	0.0008	0.0260	-1.2738	0.2122	0.6844
	RL	0.0013	0.0033	1.3297	0.2262	0.5527

(a) On validation sample

(b) On testing sample

Table C1: VaR robustness tests

D Implementation Details

This section summarizes the experimental setup for the models under study Logistic Regression (LR), Support Vector Machine (SVM), Artificial Neural Network (ANN), Multi-Layer Perceptron (MLP), Temporal Convolutional Network (TCN), and the Double Deep Q-Network (DDQN) in a reinforcement learning framework. Computations were performed on a high-performance workstation (AMD Ryzen 9 5900HX, 32 GB RAM, NVIDIA GeForce RTX 3060 GPU) using Python 3.12.8 with standard scientific libraries (NumPy, pandas, scikit-learn, PyTorch, pymc, imbens).

The data set, which covers September 1, 2008 to March 13, 2025, is based on the Euro Stoxx 50 index and related market indicators; a complete variable inventory with descriptive statistics appears in Table A1. The features selected using the Boruta algorithm were split chronologically into training, validation and test sets to avoid anticipation bias. Given substantial scale differences (Table 2), all predictors were rescaled to $[0, 1]$ using Min–Max normalization.

D.1 General Preprocessing and Training Protocol

The dataset was chronologically split into training, validation, and test subsets to preserve temporal dependence and avoid anticipation bias. Class imbalance was addressed with the ADASYN algorithm, which synthesizes minority-class observations in underrepresented regions of the feature space, thereby improving high-risk state detection. All predictors were scaled to the $[0, 1]$ range using Min–Max normalization to enhance numerical stability and accelerate convergence in gradient-based models. Model selection relied on accuracy, F1-score, recall, precision, and G-mean, with early stopping based on validation performance to prevent overfitting.

D.1.1 About Figure 1

The parameters for the ARIMA, ARIMA-GARCH, SVM and MLP models were selected through a combination of information criterion minimization (AIC / BIC) and grid search in the validation set. For time series models, ARIMA orders capture the optimal trade-off between model parsimony and predictive fit, while volatility dynamics is incorporated through the GARCH component. For machine learning models, kernel and regularization parameters for SVM and architectural depth and activation functions for MLP were tuned to maximize out-of-sample classification accuracy.

Model	Parameters	Value
ARIMA	(p, d, q)	(1, 0, 2)
ARIMA–GARCH	(p, d, q)–(P, Q)	(1, 0, 2)–(1, 1)
SVM	Kernel / C / γ	RBF / 5.82 / 0.023
MLP (Dense)	Layers / Neurons / Activation	2 / (32, 16) / ReLU

Table D1: The implementation details of Figure 1

D.1.2 Specification of Model Structures and Training Settings

This subsection reports the architectural configurations and hyperparameter settings for all models under consideration, including baseline classifiers, neural networks, temporal convolutional architectures, and the reinforcement learning framework.

Model	Parameters	ADASYN	Configuration
Logistic Regression	Regularization	Yes	L1 penalty, $l_1\text{ratio}=0.36$, $C = 3.29$
Support Vector Machine (SVM)	Kernel / C / γ	Yes	RBF kernel, $C = 10.426$, $\gamma = \text{'adaptive'}$
Single-Layer Perceptron (ANN)	Hidden units / Activation / Optimizer	Yes	41 neurons, ReLU, Adam ($lr = 0.00058$)
Multi-Layer Perceptron (MLP)	Layers / Neurons / Activation / Dropout	Yes	2 layers (41, 35), ReLU, dropout = 0.2, Adam ($lr = 0.0009$)
Temporal Convolutional Network (TCN)	Kernel size / Filters / Dropout	Yes	Kernel = 3, 64 filters, dropout = 0.1, Adam ($lr = 0.0005$)
Double Deep Q-Network (DDQN)	Network size / Discount γ / ϵ -decay	No	2 layers (96, 64), $\gamma = 0.95$, ϵ -decay = 0.995, Adam ($lr = 0.0005$)

Table D2: Summary of Model Architectures, Training Settings, and Hyperparameters

Although the complete hyperparameter optimization process implemented through Bayesian optimization required approximately 71 hours, this duration reflects a one-time calibration effort rather than a recurring operational cost. In reinforcement learning frameworks, such search procedures necessarily involve repeated model training for each candidate parameter set, which artificially inflates the reported computation time if it is not distinguished from standard training. Once optimal hyperparameters are identified, the computational burden drops substantially, with average single-run training times ranging from just a few seconds for simpler econometric or machine learning models to several minutes for deep-reinforcement learning architectures. Importantly, inference times across all models remain negligible, well below one-tenth of a second, ensuring that all approaches, including the proposed DDQN, are suitable for real-time deployment in risk monitoring systems. This separation between calibration cost and operational efficiency is essential for a fair evaluation of the practicality of the proposed methodology, particularly in institutional contexts where training is infrequent but inference is continuous.

Figure D1 reports these operational training and inference times for all benchmark models alongside the proposed DDQN framework. Training times vary considerably from one model to another, ranging from just 5 seconds for LR to 481 seconds for DDQN, reflecting the increased computational complexity of deep learning-based approaches. In contrast, inference times remain negligible for all models (less than 0.1 seconds), ensuring their practical applicability in real-time risk monitoring. DDQN, although more computationally demanding for training, maintains inference efficiency comparable to simpler models, highlighting its feasibility for operational deployment once trained.

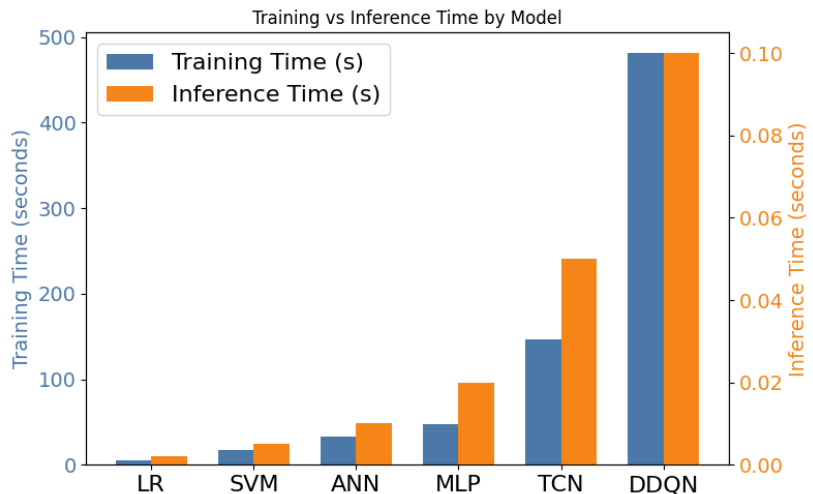


Figure D1: Average operational training times (blue bars, left Y-axis) and inference times (orange bars, right Y-axis) for all benchmark models and the proposed Double Deep Q-Network (DDQN). Reported training times exclude the one-time hyperparameter search phase (≈ 71 hours via Bayesian optimization) to reflect operational deployment conditions. Inference times remain below 0.1 seconds for all models, underscoring their suitability for real-time Value-at-Risk monitoring.